DEVELOPMENT OF A SENSITIVE ASSAY SYSTEM FOR TRITIUM RISK ASSESSMENT USING *REV1* TRANSGENIC MOUSE

Megumi Toyoshima, Hiroaki Honda, Hiromitsu Watanabe, Yuji Masuda, Kenji Kamiya

Research institute for Radiation Biology and Medicine, Hiroshima University, 1-2-3 Kasumi, Minami-ku, Hiroshima-city, HIROSHIMA, Japan, 734-8553, mtoyosh@hiroshima-u.ac.jp

Tritium, which is a radioactive isotope of the element hydrogen, would a powerful source in fuel future nuclear fusion reactors. Tritium acts much like hydrogen and is easily disbursed in environmental and biological systems. The risk assessment of tritium is one of the major issues arising in the development of the fusion reactors.

Exposure to tritium increases the risk of developing cancer as with all ionizing radiation. Cancer risk of tritium in man must be estimated based on experimental studies alone due to lack of human epidemiological data. Although the effects of tritium in mice have been described in many reports, the available information is not sufficient to accurately estimate risk from tritium exposure.

To evaluate cancer risk from tritium exposure, we developed Rev1 transgenic mice as a high radiation sensitive assay system. Rev1 has a central role in translesion DNA synthesis (TLS), which is known as error-prone DNA repair. It has been reported that absence of Rev1 sensitizes to a variety of DNA damaging agents including ionizing radiation. Overexpression of Rev1 enhanced chemical-induced tumor development in mice. From these studies, we suggest that Rev1 transgenic mouse may be a useful model system for the study of risk estimation of tritium induced cancers.

I. INTRODUCTION

Since the carbon dioxide produced by burning fossil fuels is a dominant source of anthropogenic greenhouse gas emissions, world energy systems may be changed to carbon free systems in the long run. Meanwhile energy efficiency improvements and less carbon intensive fuels such as natural gas are expected to meet urgent needs to reduce carbon dioxide emissions. Nuclear energy is expected to play a key role in the transition for achieving sustainable development. Nuclear fusion has the potential to contribute future energy systems and a cleaner environment.

If successful, fusion reactors will be the prototype for future commercial power stations, providing a cleaner and safer replacement for conventional nuclear power stations, which use nuclear fission to produce energy.

Tritium, which is a radioactive isotope of the element hydrogen, would a powerful source in fuel future nuclear fusion reactors. Because tritium acts much like hydrogen and is easily disbursed in environmental and biological systems, risk assessment of tritium is one of the major issues arising in the development of the fusion reactors.

Cancer, which is considered a stochastic effect, is the most important biological consequence of tritium exposure. As for all ionizing radiation, it has been reported that exposure to tritium increases the risk of developing cancer.[1-4] The relative biological effectiveness (RBE) value for tritium is expected to be higher than that of ionizing radiation such as X-rays and γ-rays.[1] Furthermore, the exposure conditions for tritium radiation from nuclear fusion reactor could be a long-term exposure with low dose rate. Due to lack of human epidemiological data, cancer risk of tritium in man must be estimated based on experimental studies alone. Although the effects of tritium using experimental models have been described in many reports, the available information is not enough to estimate risk from tritium exactly.

Carcinogenesis is thought to be caused by a series of mutations. Mutagenesis induced by DNA damaging agents is related to translesion DNA synthesis (TLS), which can bypass DNA lesions encountered during replication by specialized DNA polymerases such as Y-family DNA polymerases.[5,6] Although TLS permits replication of damaged templates, incorporation of mismatched bases during TLS would result in mutation.

Rev1 is the number of the Y-family DNA polymerase and has a central role in TLS pathway.[7-11] Although Rev1 can incorporate deoxycytosines opposite abasic nucleotides and some damaged guanines, it plays a regulatory, rather than a catalytic, role in error-prone TLS of other damages.[12, 13] It has been reported that hypomorphic alleles of Rev1 accelerated UV-induced tumorigenesis.[14] Furthermore, increased expression of genes involved in DNA translesion synthesis may be associated with pathogenesis of glioma.[15, 16] The mechanism of the role of Rev1 in tumorigenesis *in vivo* is still poorly understood.

We have developed *Rev1* transgenic mice to evaluate whether overexpression of Rev1 has some function on tumorigenesis. Tritium β-rays induce a variety of DNA lesions including 8-oxoguanine and abasic sites as well as single- and double- strand breaks. Rev1 can bypass these DNA lesions, as well bypass ^{6}O-methylguanine, which is the major DNA adduct formed by alkylating agents such as azoxymethane (AOM). While the DNA lesions induced by AOM are not as complicated as those induced by tritium β-rays, AOM-induced tumorigenesis provides a short-term assay for Rev1-dependent effects as compared with long-term tritium-induced cancer assays. Based on this rationale, in this study we explored whether *Rev1* transgenic mice display increased sensitivity for AOM-induced tumorigenesis. Our data indicate that overexpression of Rev1 accelerates chemical-induced tumorigenesis, and therefore may represent a sensitive model system for evaluating the effects of tritium in carcinogenesis.

II. MATERIALS AND METHODS

II.A. Animals

Female C57BL/6N mice were purchased from Charles River (Kanagawa, Japan). The development of *Rev1* Tg mice was described the submitted manuscript. Tail DNA was used for genomic PCR to determine the genotype of each mouse. The handling and sacrificing of all animals were carried out in accordance with the guidelines of the Institute of Laboratory animal Science, Hiroshima University.

II.B. Tumorigenesis experiment

Both *Rev1* Tg and normal C57BL/6N female mice were treated with 25 mM $ZnSO_4$ in drinking water beginning at 3 wk of age. Starting at 7 weeks of age, they were given weekly subcutaneous injections of AOM (15mg/ kg body weight) for 3 weeks. The mice were examined at 518 days after birth to identify any developing tumors. During the experiments, moribund mice were killed by euthanasia. Tumor tissue obtained from AOM-treated animals was collected for weight measurements and histopathology. The tumors were identified by both macroscopic and microscopic analyses.

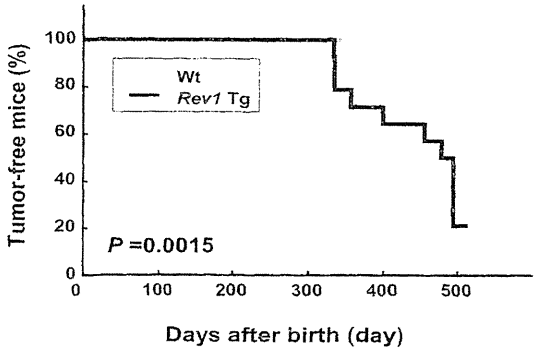

Fig. 1. Overexpressed *Rev1* accelerates AOM-induced tumorigenesis
Kaplan-Meier tumor-free survival curves of wild-type and *Rev1* Tg mice. CoxPHFit analysis showed significant difference between the two groups (P =0.0015)

II.C. Statistical Analyses

CoxPHFit was used to analyze the difference between two groups in tumorigenesis. StatMateIII was used to calculate the P value in tumor incidence between two groups. $P < 0.05$ was considered statistically significant.

III. RESULTS

AOM is known to form DNA adducts and has been recognized as a colon and liver carcinogen in rats and mice. To examine whether *Rev1* over-expression accelerates AOM-induced tumor development in mammals, we investigated a large cohort of wild-type and *Rev1* Tg female mice over an extended period to identify differences in tumor development. Wild-type and *Rev1* Tg mice were given weekly subcutaneous injections of AOM (15mg/ kg body weight) for 3 weeks and followed up for 518 days. We observed that AOM treatment increased mortality in both *Rev1* Tg and wild-type mice during this period, but the mortality rate was significantly different between the two groups (Fig. 1.). The median time of tumor-free survival was 511d for wild-type and 485d for *Rev1* Tg mice, that suggested the value in *Rev1* Tg mice was significantly shorter than that in wild-type mice.

AOM treatment induced a variety of tumors in both *Rev1* Tg and wild-type mice group. Among AOM-induced tumors, hepatocellular carcinoma was the predominate tumor type observed in both groups (Fig. 2.). Whereas the wild-type mice injected with AOM

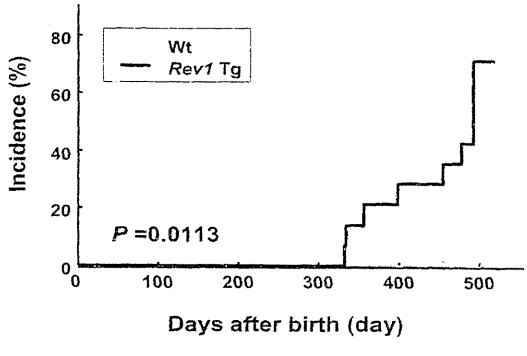

Fig. 2. *Rev1* Tg mice developed hepatocellular carcinoma at a higher incidence and a shorter latency than those of wild-type . CoxPHFit analysis showed significant difference between the two groups (P =0.0113)

developed hepatocellular carcinoma at the age of 455days, *Rev1* Tg mice injected with AOM began to develop hepatocellular carcinoma at as early as 333 days of age, 4 months earlier than wild-type mice. These data provide evidence that overexpression of Rev1 increases both the incidence of tumors and accelerates hepatic tumorigenesis induced by AOM.

Large intestinal adenomas were not detected in both groups during the time period we investigated, in spite of the fact that AOM is also known as a colon carcinogen in rodents. Aberrant crypt foci (ACF), which are putative preneoplastic lesions of colon cancer, and small intestinal adenomas were found in the large intestine of wild-type and *Rev1* Tg mice (Table 1). In wild-type mice, two adenomas were observed in the small intestines, and 13 ACF were found in the colons. On the other hand, four adenomas were found in the small intestines, and 22 ACF in the colon of *Rev1* Tg mice. There is no difference between the average number of mice with small intestinal adenoma and colonic ACF in the two groups.

The spectrum of tumor types observed in *Rev1* Tg mice was slightly different from that seen in the wild type. The difference was an increased incidence in lymphoma in the *Rev1* Tg mice. Seven of the 14 *Rev1* Tg mice developed lymphoma, whereas only two of the 9 wild-type mice did so (Table 1).

Our present data clearly indicate that overexpression of *Rev1* is in itself sufficient to predispose mice to develop other types of tumors in addition to hepatocellular carcinoma.

IV. DISCUSSION

In our previous study, we have developed *Rev1* transgenic mice and found that overexpression of *Rev1* enhanced MNU-induced tumor development.
In this study, it was explored whether *Rev1* transgenic mice are useful animal model as a high sensitive assay system for evaluating cancer risk of tritium. *Rev1* Tg mice and wild-type mice were treated with AOM as a model chemical carcinogen, as AOM is a known liver and colon carcinogen. *Rev1* Tg mice developed various types of tumors, including hepatocellular carcinoma, small intestinal adenoma, lymphoma, sarcoma and hardarian grand tumor in response to AOM exposure. Furthermore, *Rev1* Tg mice developed hepatocellular carcinoma at a higher incidence and a shorter latency than those of wild-type after AOM treatment. The incidence of AOM-induced lymphoma in *Rev1* Tg mice was higher than that in wild-type mice. From our data, overexpression of *Rev1* is sufficient to predispose mice to AOM-induced tumor with higher and shorter incidence compared with wild-type mice. Our present data clearly indicates that tumor-accelerating action of *Rev1* overexpression in mice induced by chemical carcinogens.

Although AOM induces colon cancers, there was no difference in small intestinal adenomas or colonic ACF in both wild-type and *Rev1* Tg mice groups. Development of small intestinal and colonic tumors has much longer term than that of hepatic tumor. In this study, the mice were examined at 518 days after birth to identify any developing tumors. It would be required for long period to detect the difference in the small intestinal adenomas or colonic ACF. The spectrum of tumor types observed in *Rev1* Tg mice was slightly different from that seen in the wild type. The difference was an increased incidence in lymphoma in the *Rev1* Tg mice. Expression level of Rev1 may be different in the tissue. In *Rev1* Tg mice, expression level of Rev1 in the hematopoietic tissue may be higher than that in the liver.

We have found that overexpression of Rev1 reduced cellular sensitivity to the cytotoxic effect of MNU and increased the mutagenicity of MNU, which was analyzed by measuring the frequency of HPRT mutations using human cell lines (manuscript in preparation). Furthermore, over-expressed Rev1 had the same function for radiation induced cytotoxicity and mutagenicity, respectively. Hence, as for chemical carcinogens, overexpression of Rev1 may accelerate radiation-induced carcinogenesis. It was reported that hypomorphic Rev1 accelerated UV-

TABLE 1. Tumor spectra

Organ	Wild-type (n=9)		*Rev1* Tg (n=14)	
	No. of tumors	No. of mouse with tumors (%)	No. of tumors	No. of mouse with tumors (%)
Hepatocellular carcinoma	7	7 (78 %)	11	11 (79 %)
Small intestinal adenoma	2	1 (11 %)	4	2 (14 %)
Aberrant crypt foci (ACF) in large intestine	13	5 (56 %)	22	6 (43 %)
Lymphoma	2	2 (22 %)	7	7 (50 %)
Sarcoma/ hemangiosarcoma	2	2 (22 %)	2	2 (14 %)
Hardarian grand tumor	0	0 (0 %)	2	2 (14 %)
Total	19	8 (89 %)	37	13 (93 %)

NOTE: The numbers of each tumor type and the number of animals with tumors in the indicated organs are presented. Parentheses denote tha percentage of animals with tumors in the respective organs. Total wild-type mice = 9; total *Rev1* Tg mice = 14

induced tumorigenesis.[14] Although hypomorphic Rev1 is defect in UV-induced mutagenesis, skin carcinogenesis was accelerated in these mice. This paradoxical phenotype was caused by the induction of inflammatory hyperplasia of the mutant skin that provides tumor promotion. These data suggest that expression level of Rev1 should be regulated to maintain cellular integrity.

As stated previously, risk assessment of tritium is one of the major issues arising in the development of the fusion reactors. From our data, we propose that our *Rev1* transgenic mouse model would be useful to evaluate the risk of tritium exposure in regards to carcinogenesis.

V. CONCLUSIONS

We present for the first time evidence that overexpression of *Rev1* accelarated AOM-induced tumorigenesis. Our study verifies tumor-promoting action of *Rev1* in mice. In conclusion, Rev1 transgenic mouse is thought to be useful for the study of risk estimation of tritium induced cancers.

ACKNOWLEDGMENTS

We are grateful to Hiromitsu Watanabe, Kumiko Mizuno, Teruyuki Nishioka, Masayoshi Takatani, Kazumi Shimamoto, Mai Yoshida, Tomoka Nakashima and Fumie Okubo for their assistance.

This work was supported in part by NIFS Collaborative Research Program (NIFS10KOBS015), Grants-in-Aid from the Ministry of Education, Culture, Sports, Science and Technology of Japan and by Grants-in-Aid for Cancer Research from the Ministry of Health, Labour and Welfare.

REFERENCES

1. M. P. LITTLE and B. E. LAMBERT, Systematic review of experimental studies on the relative biological effectiveness of tritium. *Radiation and environmental biophysics*, 47, 71-93 (2008).
2. O. YAMAMOTO, T. SEYAMA, H. ITOH and N. FUJIMOTO, Oral administration of tritiated water (HTO) in mouse. III: Low dose-rate irradiation and threshold dose-rate for radiation risk. *International journal of radiation biology*, 73, 535-541 (1998).
3. O. YAMAMOTO, T. SEYAMA, T. JO, H. TERATO, T. SAITO and A. KINOMURA, Oral administration of tritiated water (HTO) in mouse. II. Tumour development. *International journal of radiation biology* 68, 47-54 (1995).
4. O. YAMAMOTO, K. YOKORO, T. SEYAMA, A. KINOMURA and T. NOMURA, HTO oral administration in mice. I: Threshold dose rate for haematopoietic death. *International journal of radiation biology* 57, 543-549 (1990).
5. C. W. LAERENCE, Cellular roles of DNA polymerase zeta and Rev1 protein. *DNA repair* 1, 425-435 (2002).
6. S. D. MCCULLOCH and T. A. KUNKEL, The fidelity of DNA synthesis by eukaryotic replicative and translesion synthesis polymerases. *Cell research* 18, 148-161 (2008).
7. Y. MASUDA and K. KAMIYA, Biochemical properties of the human REV1 protein. *FEBS letters*, 520, 88-92 (2002).
8. Y. MASUDA, M. OHMAE, K. MASUDA and K. KAMIYA, Structure and enzymatic properties of a stable complex of the human REV1 and REV7 proteins. *JBC*, 278, 12356-12360 (2003).
9. Y. MASUDA, M. TAKAHASHI, S. FUKUDA, M. SUMII and K. KAMIYA, Mechanisms of dCMP transferase reactions catalyzed by mouse Rev1 protein. *JBC*, 277, 3040-3046 (2002).
10. Y. MASUDA, M. TAKAHASHI, N. TSUNEKUNI, T. MINAMI, M. SUMII, K. MIYAGAWA and K. KAMIYA, Deoxycytidyl transferase activity of the human REV1 protein is closely associated with the conserved polymerase domain. *JBC*, 276, 15051-15058 (2001).
11. C. GUO, P. L. FISHHABER, M. J. LUK-PASZYC, Y. MASUDA, J. ZHOU, K. KAMIYA, C. KISKER and E. C. FRIEDBERG, Mouse Rev1 protein interacts with multiple DNA polymerases involved in translesion DNA synthesis. *The EMBO journal*, 22, 6621-6630 (2003).
12. J. R. NELSON, C. W. LAWRENCE and D. C. HINKLE, Deoxycytidyl transferase activity of yeast REV1 protein. *Nature*, 382, 729-731 (1996).
13. J. R. NELSON, P. E. GIBBS, A. M. NOWICKA, D. C. HINKLE and C. W. LAWRENCE, Evidence for a second function for Saccharomyces cerevisiae Rev1p. *Molecular microbiology*, 37, 549-554 (2000).
14. A. TSAALBI-SHTYLIK, J. W. VERSPUY, J. G. JANSEN, H. REBEL, L. M. CARLEE, M. A. VAN DER VALK, J. JONKERS, F. R. de GRUIJL and N. DE WIND, Error-prone translesion replication of damaged DNA suppresses skin carcinogenesis by controlling inflammatory hyperplasia. *PNAS*, 106, 21836-21841 (2009).
15. H. WANG, W. WU, H. W. WANG, S. WANG, Y. CHEN, X. ZHANG, J. YANG, S. ZHAO, H. F. DING and D. LU, Analysis of specialized DNA polymerases expression in human gliomas: association with prognostic significance. *Neuro-oncology*.
16. C. H. Xi, J. HU, H. B. WANG, S. Y. ZHANG and D. L. RU, Expression study of DNA translesion synthesis genes in human primary glioma. *Zhonghua yi xue za zhi*, 89, 1309-1312 (2009).

Published online 3 October 2011

Nucleic Acids Research, 2012, Vol. 40, No. 3 ***1065–1076***
doi:10.1093/nar/gkr805

Asymmetric nature of two subunits of RAD18, a RING-type ubiquitin ligase E3, in the human RAD6A–RAD18 ternary complex

Yuji Masuda[1,*], Miki Suzuki[1], Hidehiko Kawai[2], Fumio Suzuki[2,3] and Kenji Kamiya[1]

[1]Department of Experimental Oncology, [2]Department of Molecular Radiobiology and [3]Department of International Radiation Emergency Medicine, Research Institute for Radiation Biology and Medicine, Hiroshima University, 1-2-3 Kasumi, Minami-ku, Hiroshima 734-8553, Japan

Received May 31, 2011; Revised September 7, 2011; Accepted September 13, 2011

ABSTRACT

RAD18, a RING-type ubiquitin ligase (E3) that plays an essential role in post-replication repair, possesses distinct domains named RING, UBZ, SAP and the RAD6-binding domain (R6BD) and forms a dimer. RAD6, an ubiquitin-conjugating enzyme (E2), stably associates with R6BD in the C-terminal portion. In this study, we established a method to distinguish between the two subunits of RAD18 by introduction of different tags, and analyzed mutant complexes. Our results, surprisingly, demonstrate that RAD6A and RAD18 form a ternary complex, RAD6A–$(RAD18)_2$ and the presence of only one R6BD in the two RAD18 subunits is sufficient for ternary complex formation and the ligase activity. Interestingly, ligase activity of a mutant dimer lacking both R6BDs is not restored even with large amounts of RAD6A added in solution, suggesting a requirement for precise juxtaposition via interaction with R6BD. We further show that mutations in both subunits of either RING or SAP, but not UBZ, strongly reduce ligase activity, although inactivation in only one of two subunits is without effect. These results suggest an asymmetric nature of the two RAD18 subunits in the complex.

INTRODUCTION

Ubiquitin ligases (E3s) catalyze the transfer of ubiquitin from E2 (ubiquitin-conjugating enzyme)–ubiquitin conjugates to lysine residues in target proteins. A subset of E3s contains a RING (*r*eally *i*nteresting *n*ew *g*ene) domain, which binds to E2–ubiquitin conjugates and seems to activate thioester bonds (1,2). Some RING-type E3s are known to form heterodimers such as BRCA1–BARD1 (3–5), Ring1b-Bmi1 (6,7) and MDM2–MDMX (8–10), while others like cIAP2 (11) and RNF4 (12) act as homodimers. The heterodimeric RING-type E3s are composed of active and inactive RING domains, and dimerization enhances the ligase activity, suggesting that the pairing itself is very important for enzyme function (5,6,9).

Through a RAD6-binding domain (R6BD) located in its C-terminal region, the RAD18 RING-type ubiquitin ligase forms a stable complex with a specific E2, RAD6 (13–17). Since RAD6 also contacts the RING domain near the N-terminal of RAD18 for catalytic function (2,15,18), it could interact with two distinct domains of RAD18 simultaneously. Such interactions between an E2 and an E3 are quite unique to RAD6–RAD18. Recently, it has been reported that interaction between R6BD and RAD6 blocks the intrinsic activity of RAD6 in forming ubiquitin chains, ensuring mono-ubiquitination of PCNA (19). Previous studies have also reported that RAD18 forms a dimer and suggested the RAD6–RAD18 complex to be a dimer of RAD6–RAD18 heterodimer (15,20,21), hereafter designated as $(RAD6–RAD18)_2$.

RAD6 and RAD18 play an essential role in post-replication repair of damaged DNA *via* ubiquitination of proliferating cell nuclear antigen (PCNA) at Lys164 (22,23). The RAD6–RAD18 complex itself catalyzes mono-ubiquitination of PCNA *in vitro* (24–28). The mono-ubiquitinated PCNA appears to enhance lesion bypass replication by stimulation of entry of translesion DNA polymerases at stalled 3′-ends, through interactions between ubiquitin-binding domains of the polymerases and ubiquitin moieties of mono-ubiquitinated PCNA (24,26,29–31). Furthermore, RAD18 features a pol η-binding domain that is important for recruiting pol η to stalled 3′-ends (17,32).

RAD18 has two other domains UBZ (ubiquitin-binding zinc finger) (33–35) and SAP (*S*AF-A/B, *A*cinus and

*To whom correspondence should be addressed. Tel: +81 82 257 5893; Fax: +81 82 257 5843; Email: masudayu@hiroshima-u.ac.jp

PIAS) (15,36–38). The former is required for accumulation of RAD18 at damage sites (34,37,39) and has affinity for Ub chains (33,34) suggesting specific binding to damage-associated poly-ubiquitinated proteins (39). The SAP domain possesses DNA-binding activity (15,38), although it appears to be unnecessary for accumulation of RAD18 at damage sites (37,39). Rather, it is crucial for pol η focus formation (37) possibly depending on PCNA ubiquitination, which is attributed to an essential role of the SAP domain in ligase activity (38,39).

Although multiple domains of RAD18 are clearly concerned with ligase activity, it is unknown how the distinct entities of the two RAD18 subunits interact with each other for enzyme function. In the present study, we established a method to analyze the structure and functions of the human RAD6A–RAD18 complex and demonstrated an asymmetric nature of the two RAD18 molecules in the complex.

MATERIALS AND METHODS

Plasmids

Expression plasmids for RAD6A–RAD18, E1, ubiquitin, PCNA and RFC were as described previously (26,40–42). For overproduction of human RAD6A, RAD6A–^{His}RAD18, ^{FLAG}RAD6A–^{His}RAD18, the genes were cloned into pET20b(+) (Novagen) to yield pET-RAD6A and pET-RAD6A/hisRAD18, pET-flagRAD6A/hisRAD18, respectively. To make an expression plasmid compatible with pET plasmids in *Escherichia coli* cells, the entire coding unit of pET-RAD6A/RAD18 (42) was cloned into pACYC Duet1 (Novagen) to yield pAC-RAD6A/RAD18. Expression plasmids for overproduction of RAD6A–^{FLAG}RAD18 and ^{FLAG}RAD6A–^{FLAG}RAD18, pAC-RAD6A/flagRAD18 and pAC-flagRAD6A/flagRAD18 were generated, respectively. In those plasmids, His-tagged sequences were taken from pET15 and all tagged sequences were attached to immediately before the start codons of the respective genes. Expression plasmids in human cells for *RAD6* were cloned in pCMV, and for *RAD18* in pCDNA3 flag and pCAGGS (43).

Proteins

Proteins used in this study were overproduced in *E. coli* cells. During all purification steps, monitoring was done by SDS–PAGE followed by staining with Coomassie Brilliant Blue R-250 (CBB), or western blotting. Protein concentrations were determined by Bio-Rad protein assay using BSA (Bio-Rad) as the standard. PCNA, RFC, E1, ubiquitin and RAD6A–RAD18 complex were purified as described previously (26,40,41). Detailed procedures for purification of recombinant proteins established in this study are described in Supplementary Data.

Sucrose density gradient sedimentation

Sucrose density gradient sedimentation was performed as described earlier (44). Purified RAD6A–RAD18 complexes (1.7 μg), were sedimented through 2 ml of 10–40% sucrose gradient in buffer A containing 300 mM NaCl by centrifugation at 55 000 rpm for 20 h in a TLS 55 rotor (Beckman) at 4°C and fractions (100 μl) were collected from the bottom of the tube and analyzed by SDS–PAGE. Gel bands were stained with CBB and quantified using Multi Gauge software Version 3.0 (FUJIFILM). Sedimentation coefficients were determined relative to those of standard proteins sedimented in parallel gradients.

Antibodies

To obtain polyclonal antibodies against RAD18, truncated His-tagged RAD18 proteins (127–255 amino acids) were expressed in BL21 (DE3) (45), purified and used to immunize rabbits. Anti-Penta-His monoclonal (Qiagen, 34660), anti-FLAG M2 monoclonal (Sigma, F3165), anti-RAD6 polyclonal (Abcam, ab31917) and anti-PCNA polyclonal (Santa Cruz, sc-7907) antibodies were purchased.

PCNA-mono-ubiquitination assays

The standard reaction mixture (25 μl) contained 20 mM HEPES–NaOH (pH 7.5), 50 mM NaCl, 0.2 mg/ml BSA, 1 mM DTT, 10 mM $MgCl_2$, 1 mM ATP, 100 ng poly(dA)-oligo(dT), PCNA (1 pmol), RFC (350 fmol), E1 (850 fmol), ubiquitin (170 pmol) and the indicated amounts of RAD6A–RAD18 complex. Reaction mixtures were prepared on ice then incubated at 30°C for 10 min. The reactions were terminated by addition of 2× SDS sample buffer containing 25 mM EDTA. Ubiquitination of PCNA was assessed by western analysis, detected by an ECL chemiluminescence kit (GE Healthcare Life Science).

RESULTS

Physicochemical properties of the human RAD6A–RAD18 complex

To study the subunit composition of RAD6A–RAD18 complex, we first determined the Stokes' radius and sedimentation coefficient of the purified RAD6A–RAD18 complex (26) by gel filtration and sucrose density gradient centrifugation, respectively (Table 1). The obtained value of Stokes' radius (62 Å) corresponds to an apparent molecular mass of 490 kDa, but that of the

Table 1. Physicochemical properties of the RAD6A–RAD18 complex

Stokes' radius[a] (Å)	Sedimentation coefficient[b] $\times 10^{-13}$ s ($S_{20,w}$)	Molecular mass[c] (kDa)
62	5.0	131

[a]Determined by Superdex 200 gel filtration using the size markers ferritin (61.0 Å), aldolase (48.1 Å), albumin (35.5 Å) ovalbumin (30.5 Å) and ribonuclease A (16.4 Å), and the data were based on A_{280} values monitored during the chromatography.
[b]Determined with ferritin (17.6 S), catalase (11.3 S), aldolase (7.4 S), albumin (4.2 S) and ribonuclease A (1.8 S) as standards, and the data were based on the SDS–PAGE gel profile.
[c]Estimated from the Stokes' radius and the sedimentation coefficient assuming a partial specific volume of 0.73 (46).

sedimentation coefficient (5.0 S) corresponds to an apparent molecular mass of 70 kDa. The large difference between these two values suggests that the complex does not have a compact globular shape. Employing the method described by Siegel and Monty (46), we estimated the molecular mass of the RAD6A–RAD18 complex to be 131 kDa (Table 1). Since calculated molecular masses of RAD6A and RAD18 are 17.3 and 56.2 kDa, respectively, the total of molecular mass should be 73.5 kDa for RAD6A–RAD18 and 147 kDa for $(RAD6A–RAD18)_2$. Although the value estimated from the experiments was close to that of $(RAD6A–RAD18)_2$, we further investigated the stoichiometry of RAD6A and RAD18 in the complex.

Direct evidence that the RAD6A–RAD18 complex contains two RAD18 molecules

To obtain direct evidence that the RAD6A–RAD18 complex contains two molecules of RAD18, we co-expressed both His-tagged *RAD18* and FLAG-tagged *RAD18* genes together with *RAD6A* gene in the same *E. coli* cells. Three different complexes containing ^{His}RAD18–^{His}RAD18, ^{FLAG}RAD18–^{FLAG}RAD18 or ^{His}RAD18–^{FLAG}RAD18 would be expected if we assume that the complex should contain two molecules of RAD18. When the cell lysate was loaded to a Ni-chelating column, we found some ^{FLAG}RAD18 to be absorbed to the column and eluted together with approximately equal amounts of ^{His}RAD18 at a lower imidazole concentration (Figure 1A, lane 2), whereas the remainder of the ^{His}RAD18 was eluted at a higher imidazole concentration (see Supplementary Materials and Methods section). Since it was expected that the former was ^{His}RAD18–^{FLAG}RAD18 hetero complex and the latter was ^{His}RAD18 homo complex, the former was further purified through a heparin column (Figure 1A, lane 3) and analyzed by gel filtration (Figure 1A, lane 4). The elution profile was the same as that of untagged

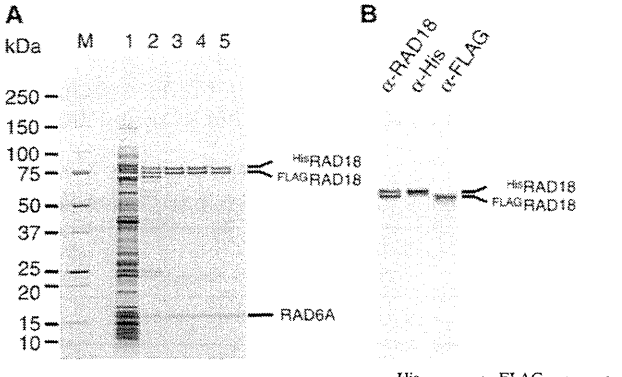

Figure 1. Purification of the RAD6A–^{His}RAD18–^{FLAG}RAD18 complex. (**A**) Pooled fractions eluted from respective columns were analyzed by SDS–PAGE followed by staining with CBB. Lane 1, cell lysate; lane 2, Ni-chelating column; lane 3, heparin column; lane 4, gel-filtration column; lane 5, anti-FLAG affinity column. Molecular masses of each marker (lane M) are shown to the left of the gel. (**B**) Western analysis of the pooled fraction eluted from the gel filtration column. Membranes were probed with the indicated antibodies.

RAD6A–RAD18 complex (Table 1 and see also Figure 6C), suggesting the tag sequences do not affect the overall structure of the complex. While western blotting with anti-Penta-His and anti-FLAG antibodies specifically detected ^{His}RAD18 and ^{FLAG}RAD18 proteins, respectively (Figure 1B), blotting with anti-RAD18 antibodies detected the two proteins equally, thereby indicating that the purified complex contains ^{His}RAD18 and ^{FLAG}RAD18 at a 1:1 ratio. To further verify that RAD6A, ^{His}RAD18 and ^{FLAG}RAD18 form a complex, a fraction eluted from gel filtration was applied to FLAG-affinity chromatography. The result demonstrated that the three proteins were adsorbed to the anti-FLAG M2 affinity gel and eluted with the FLAG peptide (Figure 1A, lane 5). We thus conclude that the RAD6A–RAD18 complex contains two RAD18 molecules.

Subunit composition of the RAD6A–RAD18 complex is RAD6A–$(RAD18)_2$

To examine the stoichiometry of RAD6A in the complex, we directly compared amounts of RAD6A in the complex with purified RAD6A protein as a reference. We applied 500 ng of the purified complex, RAD6A–^{His}RAD18–^{FLAG}RAD18, in parallel with different amounts (65 or 115 ng) of RAD6A monomers to SDS–PAGE. The amounts of RAD6A in the complex should be 65 or 115 ng, if the complex is RAD6A–$(RAD18)_2$ or $(RAD6A–RAD18)_2$, respectively (Figure 2A). The results of CBB staining and western blotting showed the amount of RAD6A in the complex to be closer to 65 ng (Figure 2A), thus suggesting that the complex contains RAD6A and RAD18 at the ratio of 1:2. To confirm this, the FLAG-tag was introduced to RAD6A and the ^{FLAG}RAD6A–^{His}RAD18–^{FLAG}RAD18 complex was purified as described above. We applied 505 ng of the purified complex to SDS–PAGE, in parallel with 500 ng of RAD6A–^{His}RAD18–^{FLAG}RAD18 as a reference (Figure 2B). Western blotting with anti-RAD6 antibodies confirmed that both complexes contained equivalent amounts of RAD6A (Figure 2B), and blotting with an anti-FLAG antibody clearly demonstrated that the molecular ratio of ^{FLAG}RAD6A and ^{FLAG}RAD18 was 1:1 (Figure 2B), suggesting strongly the ratio of RAD6A to RAD18 to be 1:2.

R6BD is located within amino acid residues 340–395 of RAD18 (Figure 3D) (17,19). Using a deletion mutant consisting of amino acid residues 1–341 of RAD18 (hereafter designated as $RAD18^{\Delta C1}$, Figure 3D), we further examined the stoichiometry of RAD6 and RAD18. When ^{His}RAD18$^{\Delta C1}$ and ^{FLAG}RAD18$^{\Delta C1}$ were co-produced with RAD6A in the same *E. coli* cells, a complex containing ^{His}RAD18$^{\Delta C1}$ and ^{FLAG}RAD18$^{\Delta C1}$ was purified similarly as described above, but it did not contain RAD6A (Figure 2C, lane 3). This result indicates that the R6BD is required for complex formation with RAD6 but is dispensable for dimerization. In contrast, when ^{His}RAD18$^{\Delta C1}$ was co-produced with ^{FLAG}RAD18 and RAD6A in the same *E. coli* cells, we successfully obtained a RAD6A–^{His}RAD18$^{\Delta C1}$–^{FLAG}RAD18 ternary complex

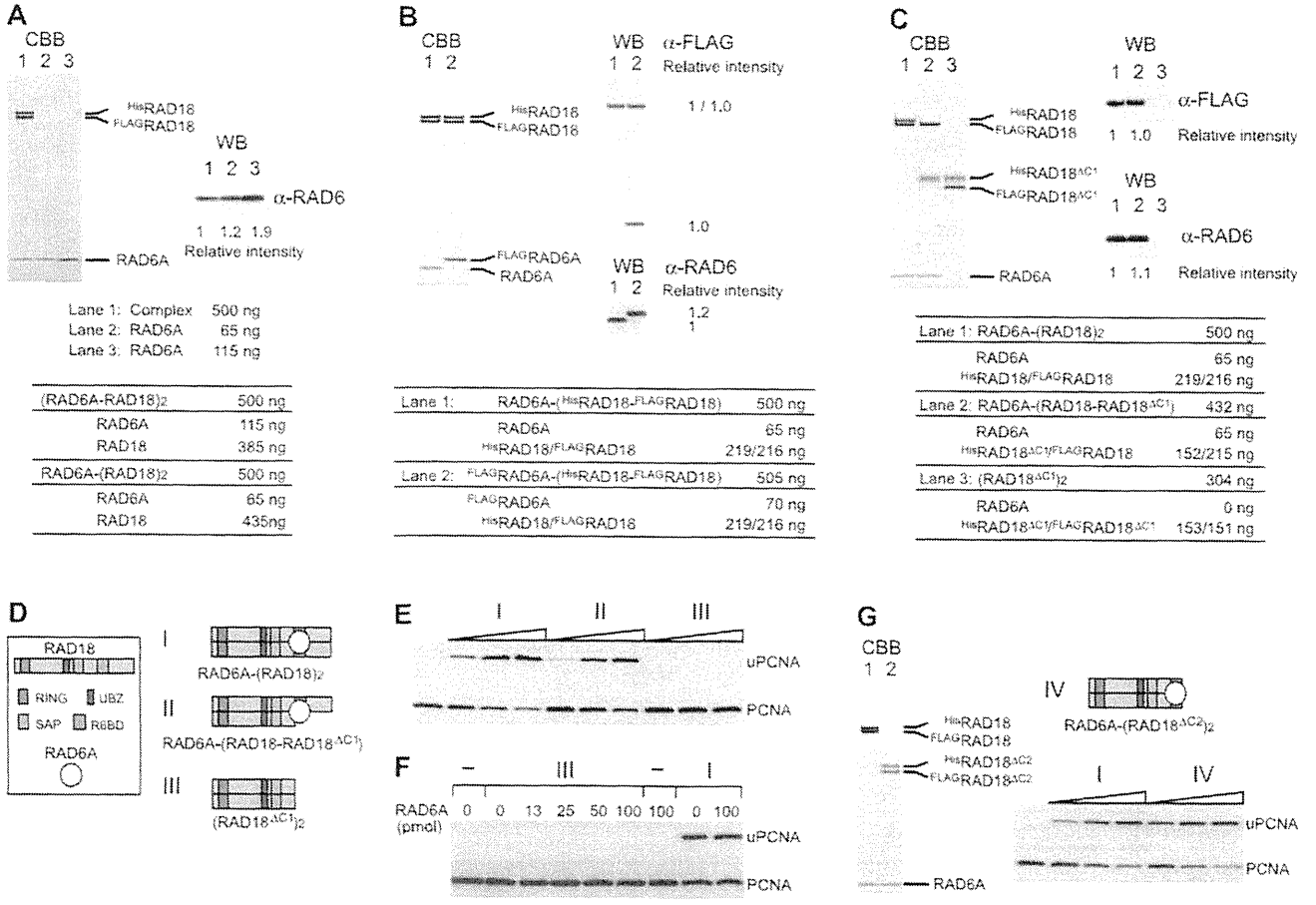

Figure 2. Subunit composition of the RAD6A–RAD18 complex and deletion analysis of RAD18. (**A**) The indicated amounts of purified RAD6A–RAD18 complex and RAD6A were analyzed by SDS–PAGE followed by staining with CBB and western blotting probed with anti-RAD6 antibodies. Relative chemiluminescence signals detected with a CCD camera are shown. Amounts of each subunit calculated for two different postulated subunit compositions are shown in the table. (**B** and **C**) Indicated amounts of purified RAD6A–RAD18 complexes were analyzed by SDS–PAGE followed by staining with CBB and western blotting probed with anti-FLAG and anti-RAD6 antibodies. Relative chemiluminescence signals detected with a CCD camera are shown. Amounts of each subunit calculated for the postulated subunit compositions are shown in the tables. (**D**) Schematic representations of the structures for respective RAD6A–RAD18 complexes. (**E**) Ligase activities of the respective RAD6A–RAD18 complexes. Increasing amounts of the complexes (0.5, 1 and 2 pmol) were subjected to standard assays. The reaction products were analyzed by western blotting with anti PCNA antibodies. I, RAD6A–(^{His}RAD18–^{FLAG}RAD18); II, RAD6A–(^{His}RAD18$^{\Delta C1}$–^{FLAG}RAD18); III, ^{His}RAD18$^{\Delta C1}$–^{FLAG}RAD18$^{\Delta C1}$. (**F**) Titration of RAD6A in the reaction with ^{His}RAD18$^{\Delta C1}$–^{FLAG}RAD18$^{\Delta C1}$. Indicated amounts of RAD6A were incubated with 2 pmol of ^{His}RAD18$^{\Delta C1}$–^{FLAG}RAD18$^{\Delta C1}$ (III) under standard assay conditions. As control reactions, 1 pmol of RAD6A–(^{His}RAD18–^{FLAG}RAD18) (I) was incubated in the presence or absence of additional RAD6A. (**G**) Analysis of complex formation and ligase activity of another C-terminal deletion mutant of RAD18. Purified complexes (3.7 pmol as a trimer) were analyzed by SDS–PAGE followed by staining with CBB. Lane 1, RAD6A–(^{His}RAD18–^{FLAG}RAD18) (I); lane 2, RAD6A–(^{His}RAD18$^{\Delta C2}$–^{FLAG}RAD18$^{\Delta C2}$) (IV). Structure of the mutant complex (IV) was represented schematically. Assays were performed as described in (E).

(Figure 2C, lane 2), indicating that only one R6BD in the two RAD18 subunits could form the complex with RAD6A. Again, amounts of each protein in these complexes were compared by CBB staining and western blotting. For Figure 2C, we applied 500 ng of RAD6A–^{His}RAD18–^{FLAG}RAD18 (lane 1) and 432 ng of the RAD6A–^{His}RAD18$^{\Delta C1}$–^{FLAG}RAD18 complex (lane 2) to SDS–PAGE. If stoichiometry of each component were 1:1:1 in both complexes, amounts of each ^{FLAG}RAD18 and each RAD6A in the two complexes should be identical (Figure 2C). The results of CBB staining and western blotting proved to be in good agreement with our estimations (Figure 2C, lanes 1 and 2), suggesting that the RAD18 dimer, as well as the RAD18 monomer, is capable of accommodating only one RAD6 molecule (Figure 2D). Very interestingly, the hetero complex RAD6A–(^{His}RAD18$^{\Delta C1}$–^{FLAG}RAD18) was catalytically active in terms of PCNA ubiquitination (Figure 2E). As expected, ^{His}RAD18$^{\Delta C1}$–^{FLAG}RAD18$^{\Delta C1}$ was inactive (Figure 2E), and its ligase activity was hardly restored by addition of excess amounts of RAD6A in solution (Figure 2F). To see whether the defect is due to the loss of function of the C-terminal portion, another truncated RAD18 mutant consisting of amino acid residues 1–388 (hereafter designated as RAD18$^{\Delta C2}$, Figure 3D), was examined. It was expected that RAD18$^{\Delta C2}$ could form a

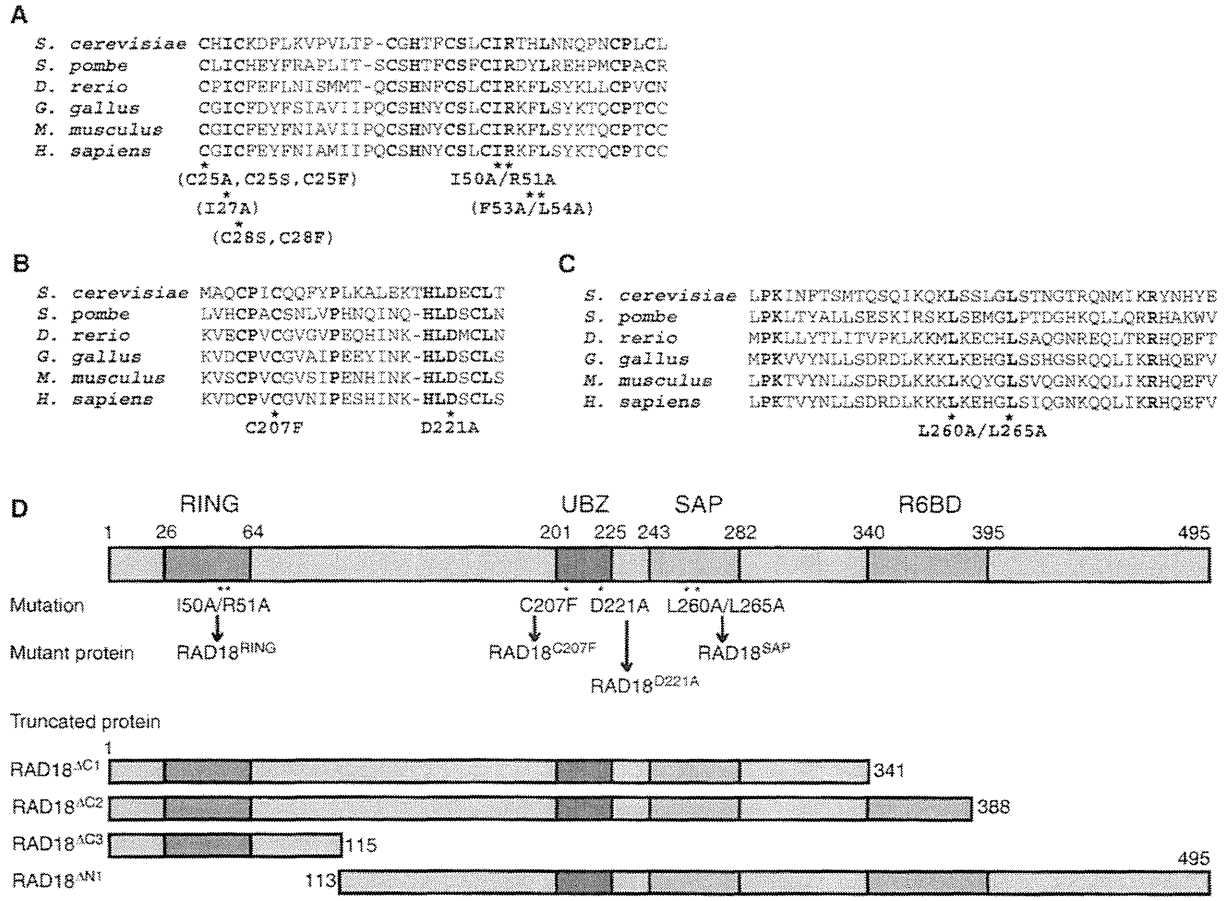

Figure 3. RAD18 mutants analyzed in this study. (**A**) Multiple alignments of the RING domains of human RAD18 and its orthologs. Mutants analyzed in this study are shown below the alignments. Mutants shown in parentheses were eluted in void volumes of gel filtration chromatography. (**B**) Multiple alignments of UBZ of human RAD18 and its orthologs. (**C**) Multiple alignments of the SAP domains of human RAD18 and its orthologs. (**D**) Schematic representations of the structures of RAD18. Positions of the mutations are shown with designated names of the mutant proteins.

complex with RAD6, since it retained R6BD (Figure 3D) (15). Indeed, it was successfully reconstituted into a ternary complex, RAD6A–^{His}RAD18$^{\Delta C2}$–^{FLAG}RAD18$^{\Delta C2}$, and the complex exhibited ligase activity similar to the wild-type level (Figure 2G), indicating that the C-terminal region of 389–495 amino acid residues is dispensable for ligase activity. From all these results (Figures 1 and 2), together with the fact that RAD6 is essentially a monomer (see Supplementary Materials and Methods section) (19,47), we conclude the subunit composition of the RAD6A–RAD18 complex to be RAD6A–(RAD18)$_2$ with a molecular mass of 130 kDa. Thus, the overall structure of the complex is asymmetric. Notably, this well matched the 131 kDa estimated molecular mass from the Stokes' radius and the sedimentation coefficient (Table 1).

Evidence of the ternary complex, RAD6A–(RAD18)$_2$, *in vivo*

To obtain evidence of ternary complex formation *in vivo*, HA-tagged *RAD6A* and FLAG-tagged *RAD18* were expressed together in human cells, and ^{HA}RAD6A–^{FLAG}RAD18 complexes were isolated using FLAG affinity and then HA affinity gels. The complexes were a mixture of unmodified RAD18 and mono-ubiquitinated RAD18, as reported previously (Figure 4A) (48). Subunit composition of the purified complexes was determined by western blotting with anti-RAD6 and anti-RAD18 antibodies using RAD6A–(RAD18)$_2$ complex purified from *E. coli* cells (26) as references. Ratio of signals from ^{HA}RAD6A and ^{FLAG}RAD18 well fitted those from RAD6A–(RAD18)$_2$ complexes (Figure 4A), suggesting the subunit composition to be RAD6A–(RAD18)$_2$. This was further confirmed using partially purified untagged RAD6A–RAD18 complexes generated by conventional column chromatography from *RAD6A* and *RAD18* expressing human cells. We found that RAD6A, RAD18 and mono-ubiquitinated RAD18 all eluted together from a gel filtration column (Figure 4B), similar to the RAD6A–(RAD18)$_2$ complex (Table 1 and Figure 6C). Again, the subunit composition of the eluted fraction corresponded to RAD6A–(RAD18)$_2$ (Figure 4B). These results strongly suggest ternary complex formation *in vivo*.

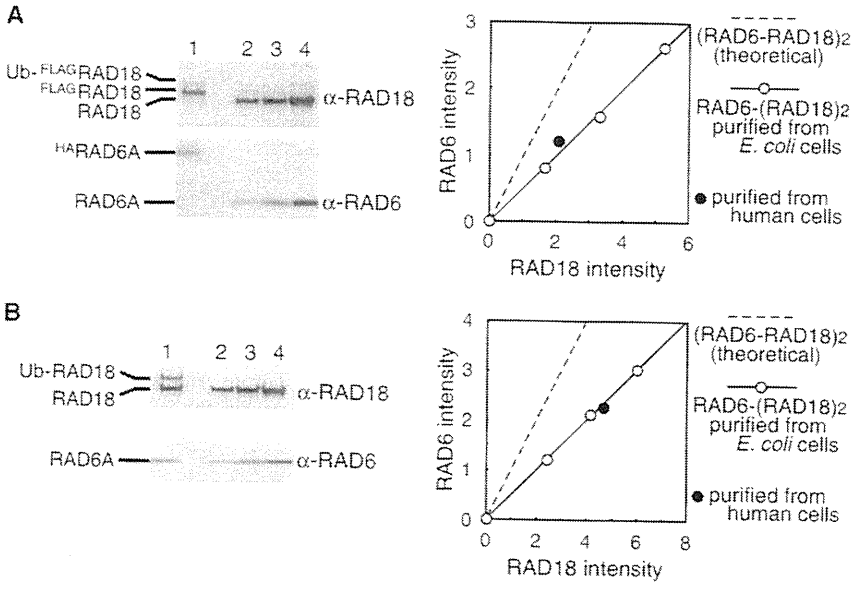

Figure 4. Ternary complex formation of RAD6A and RAD18 *in vivo*. (**A**) ^{HA}RAD6–^{FLAG}RAD18 complexes isolated from human cells were analyzed by SDS–PAGE (lane 1) together with RAD6A–(RAD18)$_2$ isolated from *E. coli* (lanes 2–4) followed by western blotting probed with anti-RAD18 and anti-RAD6 antibodies. Relative chemiluminescence signals of ^{HA}RAD6A and ^{FLAG}RAD18 (sum of unmodified ^{FLAG}RAD18 and Ub-^{FLAG}RAD18) detected with a CCD camera were plotted with those of RAD6A and RAD18 purified from *E. coli* as references. The theoretical 1:1 ratio of RAD6 and RAD18 is shown as a broken line. (**B**) Untagged RAD6–RAD18 complexes isolated from human cells were analyzed by SDS–PAGE as (A).

Analysis of UBZ roles in complex formation and ligase activity

Our system to purify RAD6–RAD18 complex with two different tags is a useful tool for analysis of structure–function relationships in RAD18. First, we applied this system to test whether UBZ is required for dimerization of RAD18 using two loss-of-function mutants, RAD18^{C207F} and RAD18^{D221A} (34,37) (Figure 3B and D). The results demonstrated that these mutants were successfully reconstituted into the complexes, RAD6A–(RAD18^{C207F})$_2$ and RAD6A–(RAD18^{D221A})$_2$ (Figure 5A) and their ligase activities were similar to that of wild-type complex (Figure 5B). These results indicate UBZ to be dispensable for complex formation and ligase activity, in line with recent reports (15,39), demonstrating reliability of our system for analysis of the structure and function of RAD6–RAD18 complexes.

Functional interaction between RAD6 and the RING domains of the two subunits of RAD18 in the complex

Next, we addressed the question whether the N-terminal part containing a RING domain mediates dimerization. We generated another truncated RAD18 mutant consisting of the 1–115 amino acid residues of RAD18 (hereafter designated as RAD18$^{\Delta C3}$, Figure 3D). When ^{His}RAD18$^{\Delta C3}$ and ^{FLAG}RAD18$^{\Delta C3}$ were co-produced with RAD6A in the same *E. coli* cells, we found the ^{His}RAD18$^{\Delta C3}$–^{FLAG}RAD18$^{\Delta C3}$ dimer to be reconstituted, but that RAD6A did not co-purify with the dimer. The observed elution profile of the dimer from a gel filtration column is shown in Figure 6A. ^{His}RAD18$^{\Delta C3}$ and ^{FLAG}RAD18$^{\Delta C3}$, confirmed by western blotting (Figure 6B), co-eluted with an apparent molecular mass of ~37 kDa, slightly larger than the calculated molecular mass of 29 kDa as a dimer (Figure 6A and B). As a complementary experiment, an N-terminal deletion mutant of RAD18 consisting of 113–495 amino acid residues (hereafter designated as RAD18$^{\Delta N1}$, Figure 3D), was generated. When ^{His}RAD18$^{\Delta N1}$ was coproduced with ^{FLAG}RAD18 and RAD6A, ^{His}RAD18$^{\Delta N1}$ co-purified with RAD6A but not with ^{FLAG}RAD18 (Figure 6D). As mentioned above, the RAD6A–(^{His}RAD18–^{FLAG}RAD18) ternary complex eluted at a position corresponding to 490 kDa in gel filtration (Figure 6C). In contrast, the complex of RAD6A–^{His}RAD18$^{\Delta N1}$ eluted at a position corresponding to 220 kDa, which is much smaller than the ternary complex (Figure 6C). Furthermore the molecular ratio of RAD6A and ^{His}RAD18$^{\Delta N1}$ determined by western blotting, compared with the ternary complex as a reference, was close to 1:1 (Figure 6D). These results suggest that the RAD6A–^{His}RAD18$^{\Delta N1}$ complex is a dimer composed of one RAD6A and one ^{His}RAD18$^{\Delta N1}$ molecule and imply that ^{His}RAD18$^{\Delta N1}$ neither self-associates nor forms a heterodimer with ^{FLAG}RAD18. From these data shown in Figure 6, we conclude that the N-terminal region (1–115) is necessary and sufficient for dimerization, while UBZ and SAP domains are dispensable.

In general, the RING domains of E3s have an essential function in ligase activity by mediating interactions with E2s (1,2). It is of great interest to clarify how the two RING domains interact with one RAD6 subunit in the RAD6A–(RAD18)$_2$ complex. To address this point, we made several mutants in which one or two conserved amino acid residues in the RING domain were replaced

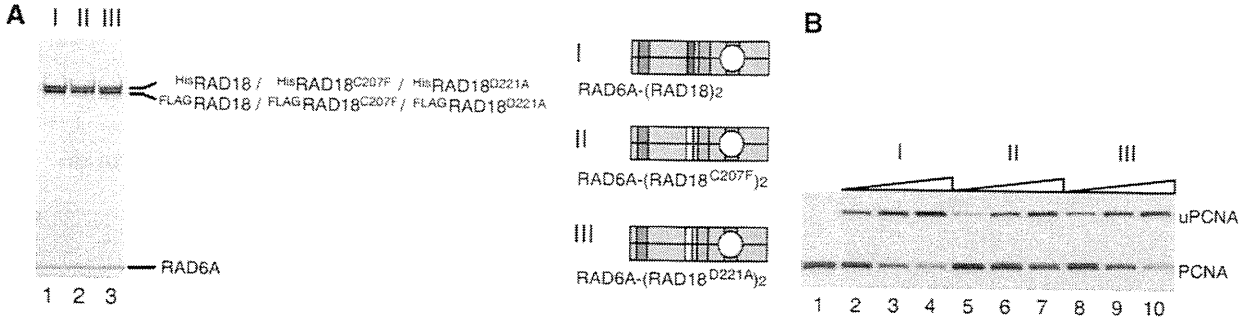

Figure 5. Analysis of ligase activity and complex formation with UBZ mutants of RAD18. (**A**) Purified complexes (3.7 pmol) were analyzed by SDS–PAGE followed by staining with CBB. I, RAD6A–(^{His}RAD18–^{FLAG}RAD18); II, RAD6A–(^{His}RAD18^{C207F}–^{FLAG}RAD18^{C207F}); III, RAD6A–(^{His}RAD18^{D221A}–^{FLAG}RAD18^{D221A}). Structures are represented schematically, UBZ domains with a mutation being shown in white boxes. (**B**) Ligase activity of the respective RAD6A–RAD18 complexes. Increasing amounts of the complexes (0.5, 1 and 2 pmol) shown in (A) were subjected to standard assays.

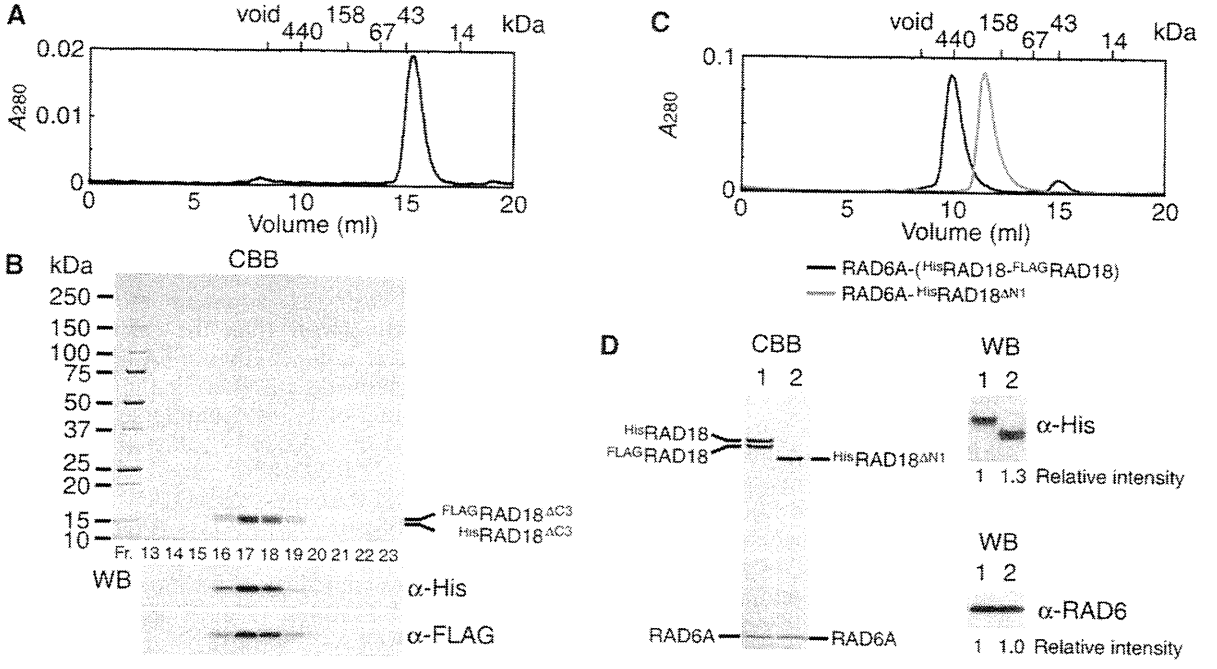

Figure 6. Analysis of RING domain for dimerization of RAD18. (**A**) Elution profile of ^{His}RAD18$^{\Delta C2}$–^{FLAG}RAD18$^{\Delta C2}$ complexes from a Superdex 200 gel filtration column. The size markers, ferritin (440 kDa), aldolase (158 kDa), albumin (67 kDa), ovalbumin (43 kDa) and ribonuclease A (14 kDa) were eluted in 10.09, 12.26, 13.74, 14.98 and 17.56 ml, respectively. The complex was eluted in 15.35 ml, estimated the apparent molecular mass of the complex to be 37 kDa from a standard curve of the marker proteins. (**B**) Analysis of fractions eluted from a Superdex 200 gel filtration column (A). Fractions between 13 and 18.5 ml were analyzed by SDS–PAGE followed by staining with CBB and western blotting probed with the indicated antibodies. ^{His}RAD18$^{\Delta C2}$ (15.1 kDa) migrated slightly faster than ^{FLAG}RAD18$^{\Delta C2}$ (14.2 kDa). (**C**) Elution profile of RAD6A–(^{His}RAD18–^{FLAG}RAD18) and RAD6A–^{His}RAD18$^{\Delta N1}$ complexes from a Superdex 200 gel filtration column. Respective complexes were eluted in 9.77 and 11.45 ml, corresponding to 490 and 220 kDa of the apparent molecular masses, and 62 and 52 Å of Stokes' radius, estimated from a standard curve of the marker proteins. (**D**) Peak fractions of gel filtration chromatography (C) were analyzed by SDS–PAGE followed by CBB staining and western blotting probed with the indicated antibodies. Relative chemiluminescence signals detected with a CCD camera are shown. Lane 1, RAD6A–(^{His}RAD18–^{FLAG}RAD18) (3.7 pmol as a trimer); lane 2, RAD6A–^{His}RAD18$^{\Delta N1}$ (3.7 pmol as a dimer).

as indicated in Figure 3A. We found that RING mutants with C25A, C25S, C25F, I27A, C28S, C27F or F53A/L54A substitutions eluted in void volumes on gel filtration chromatography, suggesting these mutants to form large aggregates due to highly disordered structures by misfolding. Therefore we did not further analyze them. However, we could successfully obtain one mutant complex containing I50A/R51A substitutions in RAD18 (hereafter designated as RAD18^{RING}, see Figures 3A and 7A, lane 2). A previous report suggested, based on the crystal structure of the c-Cbl-UbcH7 complex, that the amino acid residues Ile50 and Arg51 of RAD18 should be located in a predicted RAD6-interacting α-helix (2). Thus, it was expected that I50A/R51A mutations would affect

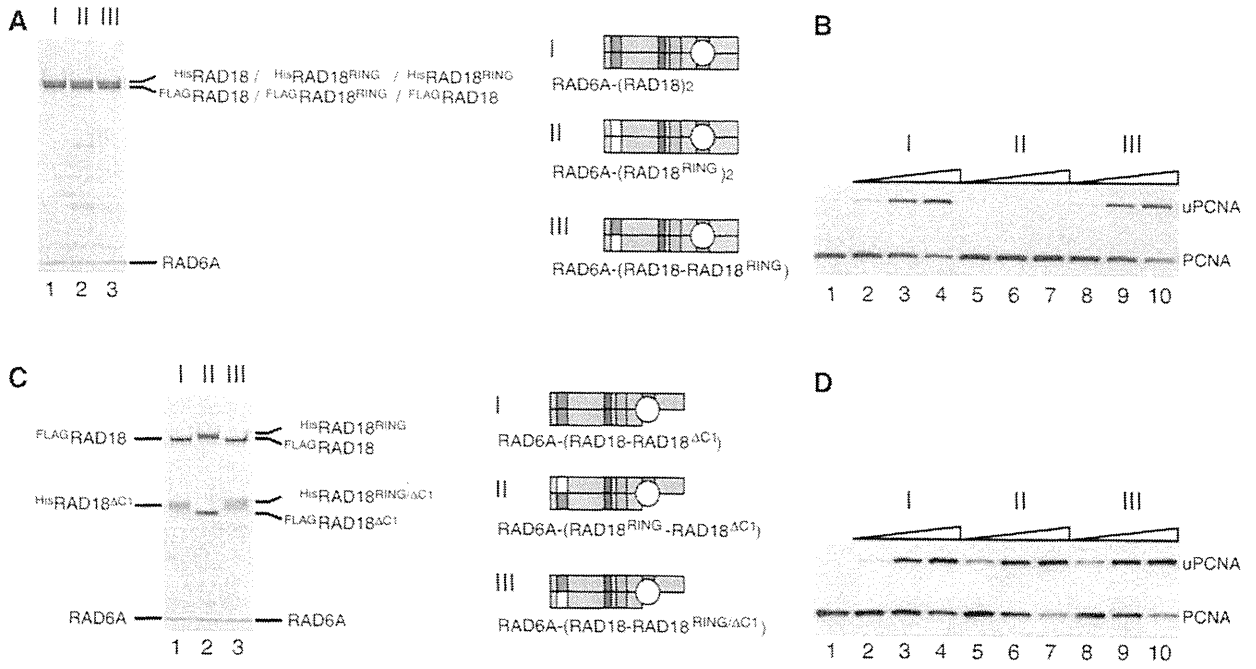

Figure 7. Analysis of ligase activity and complex formation of a RING mutant of RAD18. (**A**) Purified complexes (3.7 pmol) were analyzed by SDS–PAGE followed by staining with CBB. I, RAD6A–(^{His}RAD18–^{FLAG}RAD18); II, RAD6A–(^{His}RAD18^{RING}_^{FLAG}RAD18^{RING}); III, RAD6A–(^{His}RAD18^{RING}_^{FLAG}RAD18). Structures are represented schematically, RING domains with a mutation being shown in white boxes. (**B**) Ligase activities of the respective RAD6A–RAD18 complexes. Increasing amounts of the complexes (0.5, 1 and 2 pmol) shown in (A) were subjected to standard assays. (**C**) Purified complexes (3.7 pmol) were analyzed by SDS–PAGE followed by staining with CBB. I, RAD6A–(^{His}RAD18$^{\Delta C1}$_^{FLAG}RAD18); II, RAD6A–(^{His}RAD18^{RING}_^{FLAG}RAD18$^{\Delta C1}$); III, RAD6A–(^{His}RAD18$^{RING/\Delta C1}$_^{FLAG}RAD18). (**D**) Ligase activities of the respective RAD6A–RAD18 complexes. Increasing amounts of the complexes (0.5, 1 and 2 pmol) shown in (C) were subjected to standard assays.

the ligase activity of RAD18. In fact, it was much reduced when compared to that of the wild-type complex (Figure 7B). Then, we reconstituted a hetero complex with the mutant and wild-type, RAD6A–(^{His}RAD18^{RING}_^{FLAG}RAD18) (Figure 7A, lane 3). Surprisingly, its ligase activity was essentially identical to that of the wild-type (Figure 7B), indicating that an interaction between RAD6 and only one RING domain in the two RAD18 subunits is sufficient for ligase activity. In addition, I50A/R51A mutations were combined with the ΔC1 mutation and two mutant complexes, RAD6A–(^{His}RAD18^{RING}_^{FLAG}RAD18$^{\Delta C1}$) and RAD6A–(^{His}RAD18$^{RING/\Delta C1}$_^{FLAG}RAD18) were reconstituted (Figure 7C). Analysis of their ligase activities demonstrated these to be as active as the wild-type (Figure 7D), indicating that one RAD6 molecule in the complex has the potential to interact with either subunit of the RAD18 dimer.

Functional interaction between SAP and R6BD for ligase activity

It has been shown that the SAP domain of RAD18 has DNA-binding activity (15,38), which is separable from its essential function for ligase activity (38). When a mutant RAD18 containing L250A/L265A substitutions (hereafter designated as RAD18^{SAP}, see Figure 3D) was successfully reconstituted into the ternary complex, RAD6A–(^{His}RAD18^{SAP}_^{FLAG}RAD18^{SAP}) (Figure 8A, lane 2), the ligase activity of the mutant complex was reduced to an undetectable level (Figure 8B). However, activity was restored in a hetero complex with the wild-type, RAD6A–(^{His}RAD18^{SAP}_^{FLAG}RAD18) (Figure 8B), demonstrating that only one of the two SAP domains in the complex is sufficient for the essential SAP function. Next, the SAP mutation was combined with the ΔC1 mutation to reconstitute RAD6A–(^{His}RAD18^{SAP}_^{FLAG}RAD18$^{\Delta C1}$) and RAD6–(^{His}RAD18$^{SAP/\Delta C1}$_^{FLAG}RAD18) (Figure 8C). Interestingly, the former had quite reduced ligase activity, but the latter exhibited the wild-type level (Figure 8D), indicating that the active SAP domain should be present on the same RAD18 molecule to which RAD6 binds. In contrast, such functional interaction was not observed between RING and SAP mutants; ligase activities of RAD6A–(^{His}RAD18$^{RING/SAP}$_^{FLAG}RAD18) and RAD6–(^{His}RAD18^{RING}_^{FLAG}RAD18^{SAP}) complexes (Figure 8E) were similar to that of wild-type (Figure 8F).

DISCUSSION

In this study, we established a method to distinguish between the two subunits of RAD18 in the RAD6–(RAD18)$_2$ complex by introducing different tags at the N-termini. This enabled us to purify RAD18 complexes composed of wild–wild, wild–mutant or mutant–mutant subunits and facilitated analysis of structure–function relationships in RAD18.

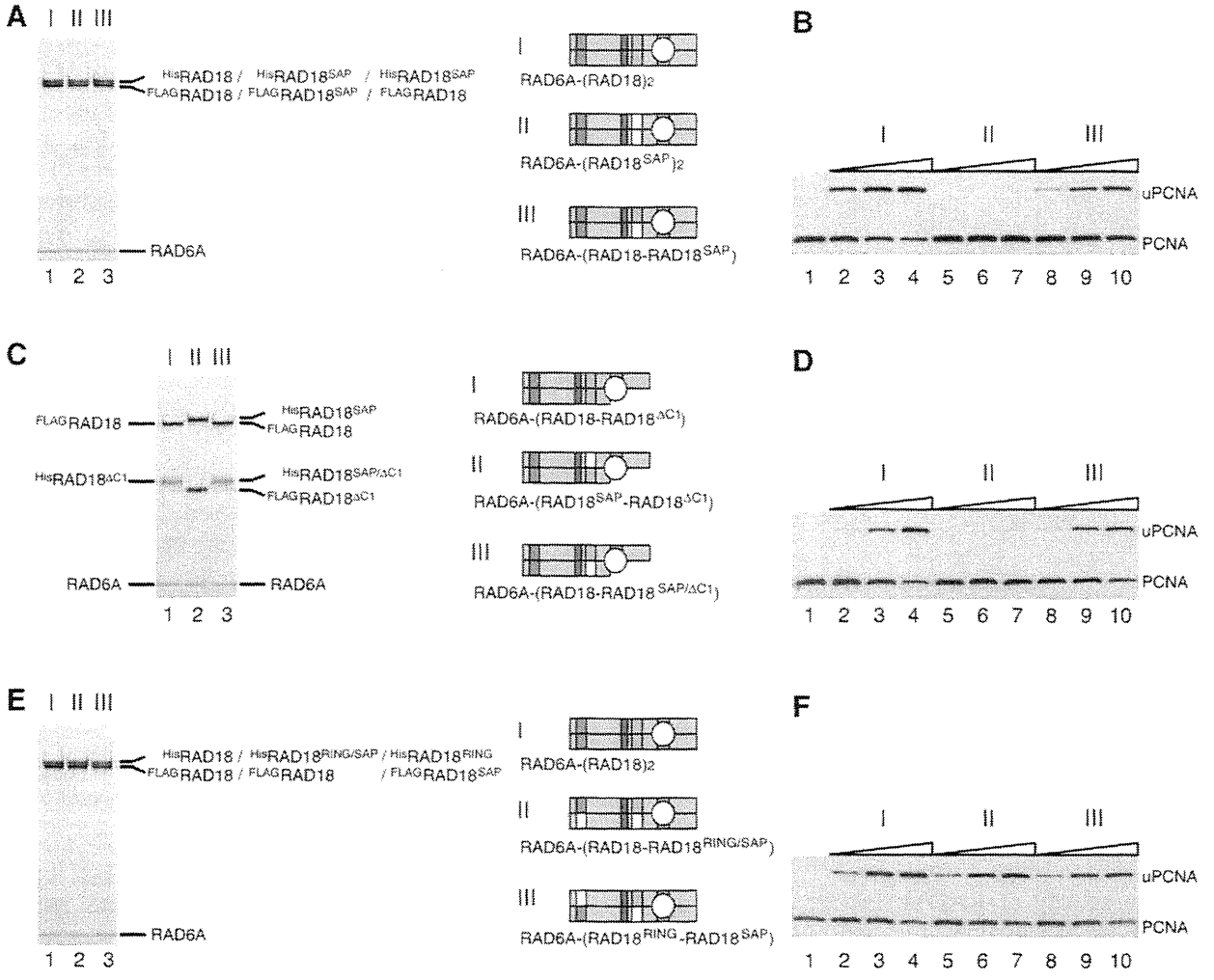

Figure 8. Analysis of ligase activity and complex formation of a SAP mutant of RAD18. (**A**) Purified complexes (3.7 pmol) were analyzed by SDS–PAGE followed by staining with CBB. I, RAD6A–(^{His}RAD18–^{FLAG}RAD18); II, RAD6A–(^{His}RAD18^{SAP}–^{FLAG}RAD18^{SAP}); III, RAD6A–(^{His}RAD18^{SAP}–^{FLAG}RAD18). Structures were represented schematically, SAP domains with a mutation being shown in white boxes. (**B**) Ligase activities of the respective RAD6A–RAD18 complexes. Increasing amounts of the complexes (0.5, 1 and 2 pmol) shown in (A) were subjected to standard assays. (**C**) Purified complexes (3.7 pmol) were analyzed by SDS–PAGE followed by staining with CBB. I, RAD6A–(^{His}RAD18$^{\Delta C1}$–^{FLAG}RAD18); II, RAD6A–(^{His}RAD18^{SAP}–^{FLAG}RAD18$^{\Delta C1}$); III, RAD6A–(^{His}RAD18$^{SAP/\Delta C1}$–^{FLAG}RAD18). (**D**) Ligase activities of the respective RAD6A–RAD18 complexes. Increasing amounts of the complexes (0.5, 1 and 2 pmol) shown in (C) were subjected to standard assays. (**E**) Purified complexes (3.7 pmol) were analyzed by SDS–PAGE followed by staining with CBB. I, RAD6A–(^{His}RAD18–^{FLAG}RAD18); II, RAD6A–(^{His}RAD18$^{RING/SAP}$–^{FLAG}RAD18); III, RAD6A–(^{His}RAD18^{RING}–^{FLAG}RAD18^{SAP}). (**F**) Ligase activities of the respective RAD6A–RAD18 complexes. Increasing amounts of the complexes (0.5, 1 and 2 pmol) shown in (E) were subjected to standard assays.

Previously, it was considered that the RAD6–RAD18 complex could be composed of two RAD6 and two RAD18, since the observations that RAD18 binds to RAD6 and it forms a dimer led to the assumption that each RAD18 molecule in the dimer should bind to RAD6 (15,20,21). However, there is little evidence for such an assignment based on the stoichiometry of RAD6. In this study, we provided hard lines of evidence that the complex is composed of one subunit of RAD6 and two subunits of RAD18, so that the overall structure of the ternary complex should be asymmetric.

The RING domains in E3s have an essential function in ligase activity by mediating interactions with E2s. Zheng *et al.* (2) have suggested, on the basis of the crystal structure of the c-Cbl-UbcH7 complex, that amino acid residues I50 and R51 in the RING domain of RAD18 are located in a predicted RAD6-interacting α-helix. Consistent with this, a mutant complex containing I50A/R51A substitutions in both RAD18 subunits exhibited severely reduced ligase activity, probably due to an impaired interaction between the altered RING domain and RAD6A. When the mutant subunit was complexed with wild-type RAD18 subunit, ligase activity was restored to the wild-type level, indicating that only one of the two RING domains is necessary for enzyme function. Furthermore, even when the RING mutation

was combined with a deletion mutation of R6BD in the same or other RAD18 subunit, the complexes exhibited robust ligase activity. These results imply that RAD6 can bind in either one of the two R6BDs, then interacting with one of the two RING domains in the RAD18 dimer.

Why should the RING domain of RAD18 form a dimer? We found that inactivation of one RING domain does not affect the ligase activity, indicating that the close proximity of two active RING domains in RAD18 is not important for the enzyme function. From our observations that some RING mutants such as C25A, C25S, C25F, I27A, C28S, C28F and F53A/L54A, probably disrupting the RING structure (Figure 3D), appeared to form large aggregates, we suggest that the RING structure is required for stable dimerization, which is in turn necessary for sustaining the functionally active RING structure of RAD18. From the results, we cannot exclude the possibility of retention of some enzyme functions even in aggregates. Indeed, it has been reported that the C28F mutant can fully complement the homologous recombination defects of RAD18-null cells (39).

The SAP domain is a unique eukaryotic module involved in sequence- or structure-specific DNA binding (36,38,49–52). Additionally, in RAD18 it has an essential role in ligase activity, separable from its function in DNA binding (38). We further demonstrated that one of the two SAP domains in the RAD6–$(RAD18)_2$ complex is sufficient for ligase activity. Interestingly, experiments using hetero complexes, in which mutation in the SAP domain was combined with a deletion mutation of R6BD, revealed an interesting relationship between SAP and R6BD. Although one of the two SAP domains and one of the two R6BDs are sufficient for enzyme activity, the active SAP domain should be present on the same RAD18 molecule to which RAD6 binds in the complex. It makes a sharp contrast to the case of RING mutant as described above. A simple explanation is that the SAP domain acts as a hinge connecting the R6BD and RING domain to enable precise juxtaposition between RING and RAD6. This might be very important for ligase activity because a deletion mutant of R6BD hardly supported PCNA ubiquitination in the presence of an excess amount of RAD6A, which should be high enough to detect ligase activities for many other E2–E3 pairs (4–6,9–2). It seems likely that binding affinity between RAD6 and the RING domain of RAD18 is very low. That could be the reason why R6BD is essential for ligase activity of the RAD6–RAD18 complex. The tight interaction between RAD6 and R6BD confers on the complex the ability to monoubiquitinate PCNA, also inhibiting the activity of RAD6 catalyzing ubiquitin chain formation (19).

In the above, we have shown that RAD6 and RAD18 forms a ternary complex, RAD6–$(RAD18)_2$ and demonstrated that one R6BD site is sufficient for the ligase activity. Then, a question that immediately arises is why RAD6 can bind to one of the two R6BD sites, but not to both of them. Although we have no experimental data to answer the question at the moment, such a case is not unprecedented. CHIP (*C*-terminal of *H*sp70 *i*nteracting *p*rotein), a protein containing a C-terminal Ubox domain (similar to RING) and an N-terminal TPR domain, forms an asymmetric dimer mediated by the Ubox domains, in which only one of the two Ubox domains is available for binding to E2 (Ubc13) because the other Ubox domain is blocked due to interaction with the TPR domain (53). It is tempting to speculate that a segment including R6BD located in a C-terminal portion of the two RAD18 subunits may interact with one of the two RING domains, consequently preventing the R6BD from interacting with RAD6. Thus, one RAD6 molecule can bind to the other R6BD and is positioned closely to another unoccupied RING domain for catalyzing the ligase function. Evidently, further experiments are required to elucidate this interesting possibility.

During the course of finally completing this manuscript, we have learned that Huang and co-workers have recently determined the structure of a RAD18 RING(1–99) dimer, also showing that this binds to RAD6 at a 2:2 ratio, whereas the full-length RAD18 dimer binds only to a single RAD6 molecule (54). Our study was conducted independently of their work.

SUPPLEMENTARY DATA

Supplementary Data are available at NAR Online: Supplementary Materials and Methods, Supplementary References [26,45,55].

ACKNOWLEDGEMENTS

The authors thank Dr Toshiki Tsurimoto (Kyushu University, Fukuoka, Japan) and Dr Tomohiko Ohta (St Marianna University School of Medicine, Kanagawa, Japan) for providing PCNA expression and ubiquitin-encoding plasmids, respectively. The authors would also like to express our appreciation to Dr Haruo Ohmori (Kyoto University, Kyoto, Japan) for his critical reading of manuscripts and valuable suggestions. The authors are grateful to Fumie Okubo, Kazumi Shimamoto and Mai Yoshida for their laboratory assistance.

FUNDING

Grants-in-Aid from the Ministry of Education, Culture, Sports, Science and Technology of Japan (to Y.M. and K.K.); Grants-in-Aid for Cancer Research from the Ministry of Health, Labour and Welfare (to K.K.). Funding for open access charge: Grants-in-Aid from the Ministry of Education, Culture, Sports, Science and Technology of Japan.

Conflict of interest statement. None declared.

REFERENCES

1. Deshaies,R.J. and Joazeiro,C.A. (2009) RING domain E3 ubiquitin ligases. *Annu. Rev. Biochem.*, **78**, 399–434.
2. Zheng,N., Wang,P., Jeffrey,P.D. and Pavletich,N.P. (2000) Structure of a c-Cbl-UbcH7 complex: RING domain function in ubiquitin-protein ligases. *Cell*, **102**, 533–539.

3. Brzovic,P.S., Rajagopal,P., Hoyt,D.W., King,M.C. and Klevit,R.E. (2001) Structure of a BRCA1-BARD1 heterodimeric RING-RING complex. *Nat. Struct. Biol.*, **8**, 833–837.
4. Hashizume,R., Fukuda,M., Maeda,I., Nishikawa,H., Oyake,D., Yabuki,Y., Ogata,H. and Ohta,T. (2001) The RING heterodimer BRCA1-BARD1 is a ubiquitin ligase inactivated by a breast cancer-derived mutation. *J. Biol. Chem.*, **276**, 14537–14540.
5. Xia,Y., Pao,G.M., Chen,H.W., Verma,I.M. and Hunter,T. (2003) Enhancement of BRCA1 E3 ubiquitin ligase activity through direct interaction with the BARD1 protein. *J. Biol. Chem.*, **278**, 5255–5263.
6. Buchwald,G., van der Stoop,P., Weichenrieder,O., Perrakis,A., van Lohuizen,M. and Sixma,T.K. (2006) Structure and E3-ligase activity of the Ring-Ring complex of polycomb proteins Bmi1 and Ring1b. *EMBO J.*, **25**, 2465–2474.
7. Satijn,D.P. and Otte,A.P. (1999) RING1 interacts with multiple Polycomb-group proteins and displays tumorigenic activity. *Mol. Cell. Biol.*, **19**, 57–68.
8. Kawai,H., Lopez-Pajares,V., Kim,M.M., Wiederschain,D. and Yuan,Z.M. (2007) RING domain-mediated interaction is a requirement for MDM2's E3 ligase activity. *Cancer Res.*, **67**, 6026–6030.
9. Linares,L.K., Hengstermann,A., Ciechanover,A., Muller,S. and Scheffner,M. (2003) HdmX stimulates Hdm2-mediated ubiquitination and degradation of p53. *Proc. Natl Acad. Sci. USA*, **100**, 12009–12014.
10. Linke,K., Mace,P.D., Smith,C.A., Vaux,D.L., Silke,J. and Day,C.L. (2008) Structure of the MDM2/MDMX RING domain heterodimer reveals dimerization is required for their ubiquitylation in trans. *Cell Death Differ.*, **15**, 841–848.
11. Mace,P.D., Linke,K., Feltham,R., Schumacher,F.R., Smith,C.A., Vaux,D.L., Silke,J. and Day,C.L. (2008) Structures of the cIAP2 RING domain reveal conformational changes associated with ubiquitin-conjugating enzyme (E2) recruitment. *J. Biol. Chem.*, **283**, 31633–31640.
12. Liew,C.W., Sun,H., Hunter,T. and Day,C.L. (2010) RING domain dimerization is essential for RNF4 function. *Biochem. J.*, **431**, 23–29.
13. Bailly,V., Lamb,J., Sung,P., Prakash,S. and Prakash,L. (1994) Specific complex formation between yeast RAD6 and RAD18 proteins: a potential mechanism for targeting RAD6 ubiquitin-conjugating activity to DNA damage sites. *Genes Dev.*, **8**, 811–820.
14. Bailly,V., Lauder,S., Prakash,S. and Prakash,L. (1997) Yeast DNA repair proteins Rad6 and Rad18 form a heterodimer that has ubiquitin conjugating, DNA binding, and ATP hydrolytic activities. *J. Biol. Chem.*, **272**, 23360–23365.
15. Notenboom,V., Hibbert,R.G., van Rossum-Fikkert,S.E., Olsen,J.V., Mann,M. and Sixma,T.K. (2007) Functional characterization of Rad18 domains for Rad6, ubiquitin, DNA binding and PCNA modification. *Nucleic Acids Res.*, **35**, 5819–5830.
16. Bailly,V., Prakash,S. and Prakash,L. (1997) Domains required for dimerization of yeast Rad6 ubiquitin-conjugating enzyme and Rad18 DNA binding protein. *Mol. Cell. Biol.*, **17**, 4536–4543.
17. Watanabe,K., Tateishi,S., Kawasuji,M., Tsurimoto,T., Inoue,H. and Yamaizumi,M. (2004) Rad18 guides polη to replication stalling sites through physical interaction and PCNA monoubiquitination. *EMBO J.*, **23**, 3886–3896.
18. Tateishi,S., Sakuraba,Y., Masuyama,S., Inoue,H. and Yamaizumi,M. (2000) Dysfunction of human Rad18 results in defective postreplication repair and hypersensitivity to multiple mutagens. *Proc. Natl Acad. Sci. USA*, **97**, 7927–7932.
19. Hibbert,R.G., Huang,A., Boelens,R. and Sixma,T.K. (2011) E3 ligase Rad18 promotes monoubiquitination rather than ubiquitin chain formation by E2 enzyme Rad6. *Proc. Natl Acad. Sci. USA*, **108**, 5590–5595.
20. Miyase,S., Tateishi,S., Watanabe,K., Tomita,K., Suzuki,K., Inoue,H. and Yamaizumi,M. (2005) Differential regulation of Rad18 through Rad6-dependent mono- and polyubiquitination. *J. Biol. Chem.*, **280**, 515–524.
21. Ulrich,H.D. and Jentsch,S. (2000) Two RING finger proteins mediate cooperation between ubiquitin-conjugating enzymes in DNA repair. *EMBO J.*, **19**, 3388–3397.
22. Friedberg,E.C., Walker,G.C., Siede,W., Wood,R.D., Schultz,R.A. and Ellenberger,T. (2006) DNA repair and mutagenesis. *2nd edn.* ASM, Washington, DC.
23. Hoege,C., Pfander,B., Moldovan,G.L., Pyrowolakis,G. and Jentsch,S. (2002) RAD6-dependent DNA repair is linked to modification of PCNA by ubiquitin and SUMO. *Nature*, **419**, 135–141.
24. Garg,P. and Burgers,P.M. (2005) Ubiquitinated proliferating cell nuclear antigen activates translesion DNA polymerases η and REV1. *Proc. Natl Acad. Sci. USA*, **102**, 18361–18366.
25. Haracska,L., Unk,I., Prakash,L. and Prakash,S. (2006) Ubiquitylation of yeast proliferating cell nuclear antigen and its implications for translesion DNA synthesis. *Proc. Natl Acad. Sci. USA*, **103**, 6477–6482.
26. Masuda,Y., Piao,J. and Kamiya,K. (2010) DNA replication-coupled PCNA mono-ubiquitination and polymerase switching in a human *in vitro* system. *J. Mol. Biol.*, **396**, 487–500.
27. Unk,I., Hajdu,I., Fatyol,K., Hurwitz,J., Yoon,J.H., Prakash,L., Prakash,S. and Haracska,L. (2008) Human HLTF functions as a ubiquitin ligase for proliferating cell nuclear antigen polyubiquitination. *Proc. Natl Acad. Sci. USA*, **105**, 3768–3773.
28. Unk,I., Hajdu,I., Fatyol,K., Szakal,B., Blastyak,A., Bermudez,V., Hurwitz,J., Prakash,L., Prakash,S. and Haracska,L. (2006) Human SHPRH is a ubiquitin ligase for Mms2-Ubc13-dependent polyubiquitylation of proliferating cell nuclear antigen. *Proc. Natl Acad. Sci. USA*, **103**, 18107–18112.
29. Bienko,M., Green,C.M., Crosetto,N., Rudolf,F., Zapart,G., Coull,B., Kannouche,P., Wider,G., Peter,M., Lehmann,A.R. *et al.* (2005) Ubiquitin-binding domains in Y-family polymerases regulate translesion synthesis. *Science*, **310**, 1821–1824.
30. Wood,A., Garg,P. and Burgers,P.M. (2007) A ubiquitin-binding motif in the translesion DNA polymerase Rev1 mediates its essential functional interaction with ubiquitinated proliferating cell nuclear antigen in response to DNA damage. *J. Biol. Chem.*, **282**, 20256–20263.
31. Zhuang,Z., Johnson,R.E., Haracska,L., Prakash,L., Prakash,S. and Benkovic,S.J. (2008) Regulation of polymerase exchange between Polη and Polδ by monoubiquitination of PCNA and the movement of DNA polymerase holoenzyme. *Proc. Natl Acad. Sci. USA*, **105**, 5361–5366.
32. Day,T.A., Palle,K., Barkley,L.R., Kakusho,N., Zou,Y., Tateishi,S., Verreault,A., Masai,H. and Vaziri,C. (2010) Phosphorylated Rad 18 directs DNA polymerase η to sites of stalled replication. *J. Cell. Biol.*, **191**, 953–966.
33. Bish,R.A. and Myers,M.P. (2007) Werner helicase-interacting protein 1 binds polyubiquitin via its zinc finger domain. *J. Biol. Chem.*, **282**, 23184–23193.
34. Crosetto,N., Bienko,M., Hibbert,R.G., Perica,T., Ambrogio,C., Kensche,T., Hofmann,K., Sixma,T.K. and Dikic,I. (2008) Human Wrnip1 is localized in replication factories in a ubiquitin-binding zinc finger-dependent manner. *J. Biol. Chem.*, **283**, 35173–35185.
35. Hofmann,K. (2009) Ubiquitin-binding domains and their role in the DNA damage response. *DNA Repair*, **8**, 544–556.
36. Aravind,L. and Koonin,E.V. (2000) SAP - a putative DNA-binding motif involved in chromosomal organization. *Trends Biochem. Sci.*, **25**, 112–114.
37. Nakajima,S., Lan,L., Kanno,S., Usami,N., Kobayashi,K., Mori,M., Shiomi,T. and Yasui,A. (2006) Replication-dependent and -independent responses of RAD18 to DNA damage in human cells. *J. Biol. Chem.*, **281**, 34687–34695.
38. Tsuji,Y., Watanabe,K., Araki,K., Shinohara,M., Yamagata,Y., Tsurimoto,T., Hanaoka,F., Yamamura,K., Yamaizumi,M. and Tateishi,S. (2008) Recognition of forked and single-stranded DNA structures by human RAD18 complexed with RAD6B protein triggers its recruitment to stalled replication forks. *Genes Cells*, **13**, 343–354.
39. Huang,J., Huen,M.S., Kim,H., Leung,C.C., Glover,J.N., Yu,X. and Chen,J. (2009) RAD18 transmits DNA damage signalling to elicit homologous recombination repair. *Nat. Cell. Biol.*, **11**, 592–603.
40. Fukuda,K., Morioka,H., Imajou,S., Ikeda,S., Ohtsuka,E. and Tsurimoto,T. (1995) Structure-function relationship of the eukaryotic DNA replication factor, proliferating cell nuclear antigen. *J. Biol. Chem.*, **270**, 22527–22534.

41. Masuda,Y., Suzuki,M., Piao,J., Gu,Y., Tsurimoto,T. and Kamiya,K. (2007) Dynamics of human replication factors in the elongation phase of DNA replication. *Nucleic Acids Res.*, **35**, 6904–6916.
42. Tomida,J., Masuda,Y., Hiroaki,H., Ishikawa,T., Song,I., Tsurimoto,T., Tateishi,S., Shiomi,T., Kamei,Y., Kim,J. *et al.* (2008) DNA damage-induced ubiquitylation of RFC2 subunit of replication factor C complex. *J. Biol. Chem.*, **283**, 9071–9079.
43. Niwa,H., Yamamura,K. and Miyazaki,J. (1991) Efficient selection for high-expression transfectants with a novel eukaryotic vector. *Gene*, **108**, 193–199.
44. Maki,H. and Kornberg,A. (1987) Proofreading by DNA polymerase III of *Escherichia coli* depends on cooperative interaction of the polymerase and exonuclease subunits. *Proc. Natl Acad. Sci. USA*, **84**, 4389–4392.
45. Studier,F.W., Rosenberg,A.H., Dunn,J.J. and Dubendorff,J.W. (1990) Use of T7 RNA polymerase to direct expression of cloned genes. *Methods Enzymol.*, **185**, 60–89.
46. Siegel,L.M. and Monty,K.J. (1966) Determination of molecular weights and frictional ratios of proteins in impure systems by use of gel filtration and density gradient centrifugation. Application to crude preparations of sulfite and hydroxylamine reductases. *Biochim. Biophys. Acta*, **112**, 346–362.
47. Worthylake,D.K., Prakash,S., Prakash,L. and Hill,C.P. (1998) Crystal structure of the *Saccharomyces cerevisiae* ubiquitin-conjugating enzyme Rad6 at 2.6 Å resolution. *J. Biol. Chem.*, **273**, 6271–6276.
48. Yuasa,M.S., Masutani,C., Hirano,A., Cohn,M.A., Yamaizumi,M., Nakatani,Y. and Hanaoka,F. (2006) A human DNA polymerase η complex containing Rad18, Rad6 and Rev1; proteomic analysis and targeting of the complex to the chromatin-bound fraction of cells undergoing replication fork arrest. *Genes Cells*, **11**, 731–744.
49. Ahn,J.S. and Whitby,M.C. (2003) The role of the SAP motif in promoting Holliday junction binding and resolution by SpCCE1. *J. Biol. Chem.*, **278**, 29121–29129.
50. Chou,C.H., Wang,J., Knuth,M.W. and Reeves,W.H. (1992) Role of a major autoepitope in forming the DNA binding site of the p70 (Ku) antigen. *J. Exp. Med.*, **175**, 1677–1684.
51. Gohring,F., Schwab,B.L., Nicotera,P., Leist,M. and Fackelmayer,F.O. (1997) The novel SAR-binding domain of scaffold attachment factor A (SAF-A) is a target in apoptotic nuclear breakdown. *EMBO J.*, **16**, 7361–7371.
52. Kipp,M., Gohring,F., Ostendorp,T., van Drunen,C.M., van Driel,R., Przybylski,M. and Fackelmayer,F.O. (2000) SAF-Box, a conserved protein domain that specifically recognizes scaffold attachment region DNA. *Mol. Cell. Biol.*, **20**, 7480–7489.
53. Zhang,M., Windheim,M., Roe,S.M., Peggie,M., Cohen,P., Prodromou,C. and Pearl,L.H. (2005) Chaperoned ubiquitylation–crystal structures of the CHIP U box E3 ubiquitin ligase and a CHIP-Ubc13-Uev1a complex. *Mol. Cell*, **20**, 525–538.
54. Huang,A., Hibbert,R.G., de Jong,R.N., Das,D., Sixma,T.K. and Boelens,R. (2011) Symmetry and asymmetry of the RING-RING dimer of Rad18. *J. Mol. Biol.*, **410**, 424–435.
55. Gomes,X.V., Gary,S.L. and Burgers,P.M. (2000) Overproduction in Escherichia coli and characterization of yeast replication factor C lacking the ligase homology domain. *J. Biol. Chem.*, **275**, 14541–14549.

Int J Hematol (2012) 95:239–245
DOI 10.1007/s12185-012-1008-y

Molecular nature of radiation injury and DNA repair disorders associated with radiosensitivity

Yuji Masuda · Kenji Kamiya

Received: 28 November 2011 / Revised: 9 January 2012 / Accepted: 9 January 2012 / Published online: 18 February 2012

Abstract Ionizing radiation (IR), as well as a wide variety of chemicals and reactive oxygen species, can cause insults in DNA integrity. However, IR is distinct from other agents in that produces clustered DNA damage, particularly double-strand DNA breaks (DSBs). The discovery of radiosensitive human diseases has revealed that the molecular mechanisms underlying the biological effects of IR impact cellular responses to and repair of DSBs. One class of diseases, including ataxia-telangiectasia, displays a defect in checkpoint response to DSBs. Another class of diseases exhibits severe combined immunodeficiency and defects in DSB repair. Importantly, radiosensitive human diseases are also associated with increased risks of leukemia/lymphoma. In this review, we summarize the molecular nature of IR-induced DNA damage, and provide an overview of the molecular mechanisms of checkpoint response to and repair of DSBs. Lastly, we discuss the roles of these mechanisms in the development of the immune system and the suppression of lymphoma/leukemia, based on the clinical features and experiments with model mice.

Keywords Ionizing radiation · Double-stranded DNA breaks · Ataxia-telangiectasia · Severe combined immunodeficiency · Non-homologous end-joining

Y. Masuda
Department of Genome Dynamics, Research Institute of Environmental Medicine, Nagoya University, Furo-cho, Chikusa-ku, Nagoya 464-8601, Japan

Y. Masuda · K. Kamiya (✉)
Department of Experimental Oncology, Research Institute for Radiation Biology and Medicine, Hiroshima University, 1-2-3 Kasumi, Minami-ku, Hiroshima 734-8553, Japan
e-mail: kkamiya@hiroshima-u.ac.jp

Introduction

Ionizing radiation (IR) produces a wide variety of oxidative DNA damage. Cells recognize the damage and activate signal transduction pathways and repair systems to protect cells from such injury. The discovery of a radiosensitive human disease [1] has stimulated studies on the molecular mechanisms underlying the biological effects of IR. Now we recognize that the mechanisms; namely, checkpoint response to and repair of double-stranded DNA breaks (DSBs), have very important roles not only in the protection of cells from IR, but also in the development, aging, immune system and tumor suppression. In this review, we introduce the molecular nature of IR-induced DNA damage in comparison with chemicals damage. Then, we discuss roles of the checkpoint response and the repair mechanism in the development of the immune system and the suppression of lymphoma/leukemia, based on clinical features and experiments with model mice.

Damage to DNA by endogenous and environmental insults

DNA is a stable biomacromolecule. Even though *N*-glycosyl bonds with purine bases are relatively unstable, the frequency of hydrolysis of the *N*-glycosyl bonds in DNA molecules, producing abasic sites, is once per 1,000 years. Deamination of cytosine, producing uracil, occurs once per 70,000 years [2]. However, such rare events are significant in terms of maintaining genetic information. Because the genome size of humans is 3×10^9 base pairs, approximately 300 abasic sites and 4 uracils are estimated to be produced in 1 h in one human cell. Furthermore, targets of such hydrolytic and oxidative damage are naturally present

in DNA, i.e. carbons and nitrogens of bases and deoxyribose, and phosphodiester bonds [3]. The primary oxidative compounds are further decayed to many different chemical species because of their instability. Thus, many kinds of oxidative damage can be produced, and nearly 100 different types of oxidative damage have been identified [4, 5]. It has been estimated that oxidative damage causes the turnover of 2,000–10,000 purine bases per day in one human cell [6]. In addition to oxidative DNA damage, nucleophilic centers of bases, almost all oxygens, nitrogens, except for *N*-glycosyl bonds, as well as phosphates are targets of alkylation [7]. Many metabolic intermediates including *S*-adenosylmethionine (SAM) can be endogenous alkylating agents. Thus, many kinds of alkylating damage are also produced in cells. Reaction mechanisms of oxidation and alkylation of DNA are reviewed in detail [4, 7].

IR and environmental chemicals insult DNA as endogenous reactive species, producing oxidative DNA damage and introducing adducts to DNA, respectively. For example, benzo[*a*]pyrene, a carcinogen from cigarette smoking, and aflatoxin, a carcinogen produced by fungi, make adducts to the 2-amino position and N7 position on guanine, respectively [7, 8] and such DNA damage is specific to environmental chemicals. In contrast, oxidative DNA damage by IR can be also produced by endogenous reactive oxygens, already present in un-irradiated cells. The total amount of oxidative DNA damage produced in un-irradiated human cells in 1 day is estimated to correspond to that produced by 10 Gy of γ-ray irradiation with a dose rate of 7 mGy/min, which is roughly comparable to 7 mSv/min [9]. The amount of damage from environmental exposure of IR (1 mSv/year) is far less than the endogenous damage level.

The estimation of the amount of oxidative damage as above-mentioned seems to be somehow curious, because we are quite healthy even with the presence of similar amounts of oxidative damage to that produced by chronic irradiation of 7 mGy/min. A specific property distinguishing IR from endogenous oxygen species must be present. The most important such property of IR is the production of clustered DNA damage, especially DSBs. Because oxidation of deoxyribose causes strand breaks, damage to two sugars in opposite strands produce DSBs. One Gy of γ-ray irradiation to human cells produces 16–40 DSBs in addition to 600–1,000 single-stranded breaks (SSBs) [9, 10]. As a consequence, the lethal effect of IR is attributed to DSBs. This notion is supported by defective DNA repair mechanisms in cells from patients with radiosensitive diseases (see below).

Chemical structures of strand breaks in DNA

Strand breaks arise by abstraction of hydrogen atom from deoxyribose (Fig. 1a). Abstraction of H can occur at C2′, C3′, C4′ and C5′ positions [4]. The base attached to the damaged sugar is released in all cases, and some fragment of the deoxyribose moiety remains at the 5′ or 3′ break end (Fig. 1b) [4]. This indicates that the template strand for the missing base is required for accurate repair synthesis after trimming of break ends to produce 3′-OH for primer and 5′-phosphate for ligation (Fig. 1c) [11]. In the case of SSBs, the damage is repaired easily because of the presence of the opposite template strand. Contrarily, in the case of DSBs, it is easy to imagine that accurate repair synthesis is impossible because the two proximate bases located in the opposite strands are missing. Thus, direct re-joining of the DSB has the probability of loss of genetic information. If the DSB is repaired by homologous recombination, such risk could be negligible.

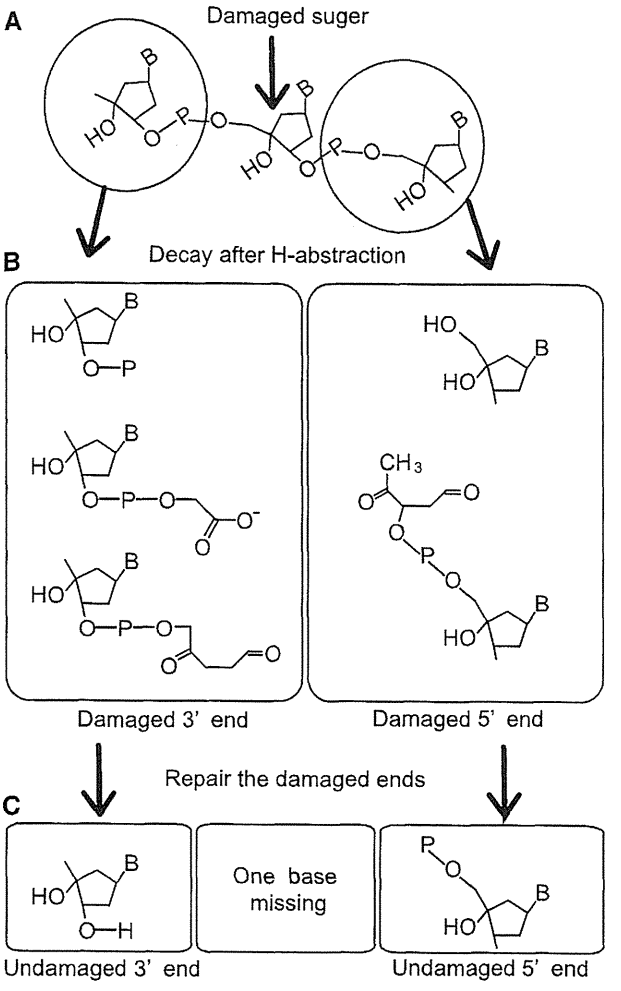

Fig. 1 Schematic representation of sugar damage in DNA. **a** Strand breaks are initiated by abstraction of hydrogen atom from deoxyribose. **b** Examples of chemical structures of the break ends. **c** Undamaged break ends after repair processing

Radiosensitive diseases

A disorder characteristic of radiosensitive disease has been discovered in the course of treatment for lymphosarcoma that developed in a patient with ataxia-telangiectasia (AT) [1]. After irradiation to the tumor site, the patient developed severe dermatitis and deep tissue necrosis resulting in death in 8 months [1]. The clinically observed radiosensitivity of AT patients [1, 12] was demonstrated to be a defect at the cellular level [13]. Subsequently, many syndromes associated with radiosensitivity, the Nijmegen breakage syndrome (NBS) [14], ataxia-telangiectasia-like disorder (ATLD) and Nijmegen breakage syndrome-like disorder (NBSLD) have been reported [15–18]. These syndromes have phenotypic characteristics similar to AT at the cellular level. To date, genes responsible for the disorders have been identified as *ATM* for AT, *NBS1* for NBS, *MRE11A* for ATLD and *RAD50* for NBSLD [18–22]. Importantly, these gene products are all required for checkpoint response, a signal transduction pathway that senses DSBs (see below).

In addition, another class of disorders with severe combined immunodeficiency (SCID) is also associated with radiosensitivity, and the responsible genes have been identified as *DNA-PKcs*, *Artemis* and *LIG4* (DNA ligase IV) [23–26]. Notably, these gene products are all involved in the repair process, non-homologous end-joining (NHEJ), of DSBs induced by RAG proteins as well as IR (see below).

Cell biological properties

The cell biological characteristics of AT, NBS, ATLD and NBSLD are all similar. In addition to radiosensitivity, they are sensitive to radiomimetics like bleomycin and a wide variety of DNA damaging agents. In the early days, it had been generally considered that the primary defect in AT is a DNA repair defect. However, an obvious DNA repair defect has not been observed [13]. Rather, AT cells exhibit characteristics of radioresistant DNA synthesis (RDS) so that RDS has been used as a diagnostic marker for AT [27, 28]. This property is also observed in NBS [29–32], ATLD [22] and NBSLD cells [18]. In normal cells, replicative DNA synthesis is inhibited by IR as a consequence of checkpoint response. This property of RDS strongly suggests a defect of the checkpoint function in AT, NBS, ATLD and NBSLD cells. However, several reports have suggested that the sensitivity of those cells is not explained by only a defect of checkpoint response [33]. More recently, it has been recognized that ATM has a function to enhance homologous recombination at the damage sites by recruitment of repair enzymes (see below).

Cells deficient in *DNA-PKcs*, *Artemis* and *LIG4* all do show normal radiation induced cell cycle checkpoint response, and thus the radiosensitivity can be attributed to impaired NHEJ [34]. Patients with a defect in NHEJ are rather characteristic of SCID (see below).

Molecular functions

DNA damage response is initiated from recognition of specific DNA damage by sensor proteins (Fig. 2). For DSBs, MRE11A–RAD50–NBS1 (MRN) complex initially recognizes the DSB end, and recruits and activates ATM via specific interaction with NBS1 [19, 35, 36]. ATM is a member of the phosphoinositide 3-kinase (PI3K)-related protein kinase (PIKK) family of serine/threonine protein kinases [20]. ATM phosphorylates more than 700 proteins containing the phosphorylation motif (SQ/TQ) in response to IR [37], including MRN complex, a histone variant, H2AX, a checkpoint mediator, MDC1, a checkpoint kinase, CHK2 and p53. Phosphorylations of MRN complex, H2AX and MDC1 initiate recruitment of many factors required for signal transduction and homologous recombination, enhancing the repair process [38–42]. It has been considered that a marginal repair defect observed in AT cells [33] might reflect the reduced efficiency of homologous recombination. The cell cycle is arrested at the G1 phase through phosphorylation of CHK2 and activation of p53 (Fig. 2) [39, 43, 44].

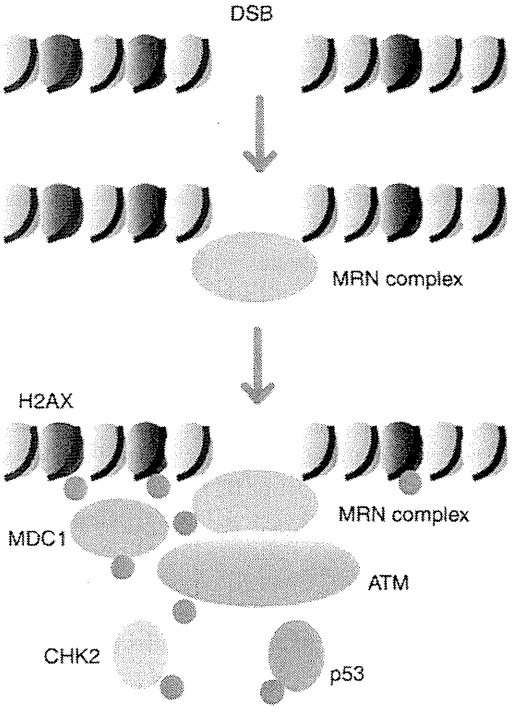

Fig. 2 DNA damage response to DSBs

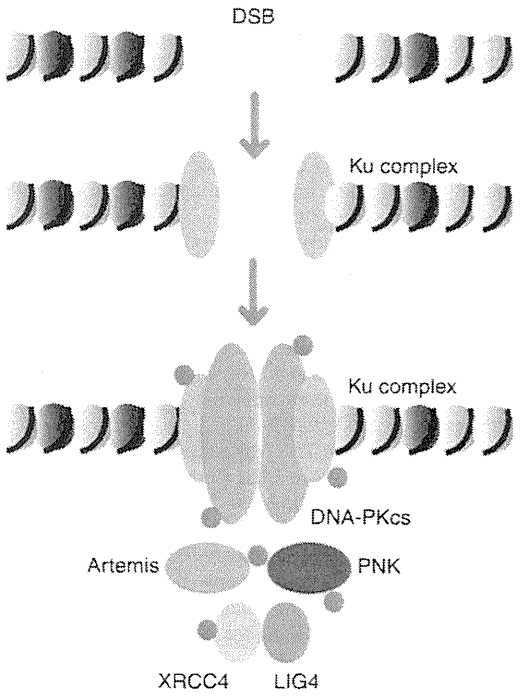

Fig. 3 NHEJ of DSBs

DSB repair through NHEJ is initiated by binding Ku70–Ku80 complex to the break ends (Fig. 3). The Ku complex recruits and activates DNA-PKcs via specific interaction with Ku80 [35]. DNA-PKcs is also a member of PIKK family [45], but its contribution to checkpoint response is insignificant. Rather, it phosphorylates multiple proteins involved in NHEJ [46]. *Artemis*, a nuclease, and PNK, a kinase/phosphatase, process the ends [11, 47, 48], and DNA ligase IV, a complex with XRCC4, ligates two DSB ends (Fig. 3) [49, 50].

Immunological disturbances and etiological aspects

In patients with AT, NBS and ATLD, immune deficiency is observed in the humoral immune system. IgA and IgG deficiency can be found [51–57]. B cells from patients have an intrinsic defect in maturation from IgM to other classes, as evidenced by normal or raised IgM. This suggests a defect in class switch recombination (CSR). This assumption has been documented at the molecular level using genomic DNA purified from peripheral blood cells from patients with AT, NBS and ATLD [58, 59]. Furthermore, the gene functions of *Atm* [60, 61] and *Nbs1* [62, 63] for CSR are confirmed by genetically engineered model mice. However, the molecular link between CSR and ATM pathway is currently unknown.

Patients with mutations in *DNA-PKcs*, *Artemis* and *LIG4* all show $T^-B^-NK^+$ SCID phenotype [23, 24, 64, 65]. Absence of mature B and T cells, but the presence of NK cells is characteristic of defects in V(D)J recombination. Mutations in RAG1 or RAG2 genes, encoding a lymphoid-specific endonuclease, also give rise to $T^-B^-NK^+$ SCID. The involvement in V(D)J recombination has been also demonstrated by model animals for *DNA-PKcs* [66–68], *Artemis* [69] and *LIG4* [70]. Therefore, SCID phenotype is attributed to the defect in the end-joining process after break induction by RAG proteins.

Increased risks of leukemia/lymphoma and etiological aspects

AT patients have a high risk of developing leukemia/lymphoma, which includes both B and T cell tumors, but not myeloid tumors. Incidence of childhood T cell lymphoma and T-ALL is greatly increased, although no differences between tumors in non-AT children are observed. In young adult AT patients, susceptibility to T cell prolymphocytic leukemia (T-PLL) is obvious. It is quite a contrast to non-AT patients who develop T-PLL with a median age of 69 years. However, no differences between AT and non-AT patients have appeared in clinical settings. Analysis of chromosome translocation associated with T-ALL and T-PLL reveals an involvement of a TCR gene. The translocation is attributed to irregular rejoining after processing with RAG proteins. It is characteristic to T-ALL and T-PLL in non-AT patients (reviewed in [71]). These clinical features imply two possibilities to explain the high incidence of lymphoma/leukemia in AT patients: early onset of tumorigenesis could be associated with an increased number of abnormal re-joining at V(D)J recombination sites and/or increased genetic instability accelerates tumorigenesis of the particular cell which has this rearrangement. The two possibilities are mutually not exclusive. In addition, there is no evidence that the susceptibility is attributed to immunodeficiency in AT patients. Importantly, evidence from model mice is striking [72]. $Atm^{-/-}$ mice are highly susceptible to thymic lymphoma. However, it is largely suppressed in $Atm^{-/-}$ and $Rag1^{-/-}$ double knock out mice. This is consistent with the idea that RAG-induced DSBs are the primary factor for the higher incidence of lymphoma/leukemia, even though any contribution of genetic instability to accelerate tumorigenesis could not be formally excluded in AT patients.

NBS patients are susceptible to lymphoma. In most cases, non-Hodgkin's lymphomas (NHL) develop [73]. Because the risk for NHL is increased by immunosuppressive therapy [74], the high incidence of NHL in NBS patients could be attributed to their immunodeficiency.

Although only a limited number of patients with a defect in NHEJ have been reported, susceptibility to leukemia/